

**SEARCHING FOR Bi³⁺ PEROVSKITE OXYHALIDES:
EXAMINING THE RELATIONSHIP
BETWEEN STABILITY AND BISMUTH
LONE PAIR HYBRIDIZATION**

by

Richard M. Egan

A thesis submitted to the Faculty of the University of Delaware in partial fulfillment of the requirements for the degree of Honors Bachelor's of Chemical and Biomolecular Engineering with Distinction

Spring 2018

© 2018 Richard M. Egan
All Rights Reserved

**SEARCHING FOR Bi³⁺ PEROVSKITES OXYHALIDES:
EXAMINING THE RELATIONSHIP
BETWEEN STABILITY AND BISMUTH
LONE PAIR HYBRIDIZATION**

by

Richard M. Egan

Approved: _____
Douglas Buttrey, Ph.D.
Professor in charge of thesis on behalf of the Advisory Committee

Approved: _____
Ismat Shah, Ph.D.
Committee member from the Department of Material Science &
Engineering

Approved: _____
Susan Groh, Ph.D.
Committee member from the Board of Senior Thesis Readers

Approved: _____
Paul Laux, Ph.D.
Director, University Honors Program

ACKNOWLEDGMENTS

I take this space to recognize the support of Dr. Buttrey, for his patience and investment in me as a researcher. By taking the time to explain the tenets of crystallography, x-ray diffraction, and solid-state chemistry, he has inspired me to learn more while providing me with the tools to do so. I would also like to thank Drs. Groh and Shah for their advice and suggestions in presenting and directing this work. This section would not be complete without mentioning the help of my fellow colleague, Lencho Amente, whose support, suggestions, and genuine interest helped me to push through tough obstacles. Finally, I would like to thank my family. I am not the first person in my family who wanted to go to college, but I am the first one who got to, and for that I will forever be indebted to them.

TABLE OF CONTENTS

LIST OF TABLES	vi
LIST OF FIGURES	vii
ABSTRACT	xi
CHAPTERS	
1 INTRODUCTION	1
MOTIVATION.....	1
PEROVSKITE UNIT CELL	5
TOLERANCE FACTOR.....	6
LONE PAIR ELECTRON HYBRIDIZATION	11
HYPOTHESIS.....	11
2 PRECALCULATIONS	13
FIRST-PRINCIPLES LATTICE CONSTANT PREDICTIONS	13
XRD SPECTRA PREDICTIONS	18
HYPOTHETICAL UNIT CELL	19
3 EXPERIMENTAL METHODS	22
REAGENTS	22
BISMUTH OXYCHLORIDE SYNTHESIS.....	22
CESIUM CHLORIDE HANDLING.....	23
SAMPLE SYNTHESIS.....	23
CRUCIBLE CLEANING.....	24
SAMPLE CHARACTERIZATION.....	24
EXPERIMENTAL CONDITIONS	25
4 REAGENT XRD PATTERNS.....	27
BISMUTH OXYCHLORIDE	27
METHYLAMMONIUM CHLORIDE.....	27
CESIUM CHLORIDE.....	28
5 PRODUCT XRD PATTERNS.....	29
EXPERIMENTS 5, 7a, & 7b.....	29
EXPERIMENTS 6, 8a, & 8b.....	31
EXPERIMENTS 12, 17, 18, & 19	33
EXPERIMENTS 24, 25a, 25b, & 25c	35
EXPERIMENTS 26a & 26b.....	37

EXPERIMENTS 27, 28, 29, & 30	39
6 DISCUSSION.....	41
7 CONCLUSIONS	43
REFERENCES	45
APPENDICES	
A APPENDIX A: EXCEL LATTICE CONSTANT FITTING.....	50
EXPERIMENT 6.....	50
EXPERIMENT 7b.....	51
EXPERIMENT 8a.....	51
EXPERIMENT 8b.....	52
EXPERIMENT 24.....	53
EXPERIMENT 25a.....	54
EXPERIMENT 25b.....	56
EXPERIMENT 25c	58
EXPERIMENT 30.....	60
B APPENDIX B: X-RAY DIFFRACTION SPECTRA	62
EXPERIMENT 5.....	62
EXPERIMENT 7a.....	62
EXPERIMENT 7b.....	63
EXPERIMENT 6.....	63
EXPERIMENT 8a.....	64
EXPERIMENT 8b.....	64
EXPERIMENT 12.....	65
EXPERIMENT 17.....	65
EXPERIMENT 18.....	66
EXPERIMENT 19.....	66
EXPERIMENT 24.....	67
EXPERIMENT 25a.....	67
EXPERIMENT 25b.....	68
EXPERIMENT 25c	68
EXPERIMENT 26a.....	69
EXPERIMENT 26b.....	69
EXPERIMENT 27.....	70
EXPERIMENT 28.....	70
EXPERIMENT 29.....	71
EXPERIMENT 30.....	71

LIST OF TABLES

Table 1	Calculation of the predicted dimension length derived from the length of each contact axis of the hypothetical methylammonium bismuth oxyhalide octahedra.....	13
Table 2	A summarization of the predicted lattice parameters for the hypothetical compounds of interest. Green, red, purple, and blue shading refers to the oxygen, chlorine, bromine, and iodine contributions, respectively.....	14
Table 3	Lattice parameters calculated for arbitrary angles of tilt in the specified perovskite octahedron. The origin of the tilting angle was taken to be the B-site of the unit cell.....	17
Table 4	Peak angles for six hypothetical bismuth oxyhalide compounds were calculated from the predicted lattice constants found for perovskites containing the respective atom, assuming no tilting of the octahedron. .	18
Table 5	Summary of pertinent experimental factors in laboratory attempts to synthesize the perovskite compounds of interest. (*)-marked experiments are meant to indicate that silicon standard was added to check the calibration of the XRD instrument. Greyed out experiments were not analyzed due to contamination or believed to not be insightful.....	26
Table 6	Summary of the lattice constants derived for one phase found in four samples heated at the same temperature and composition for varying amounts of time.	36

LIST OF FIGURES

Figure 1	Depiction of an B-site centered perovskite unit cell. The A-site cation is marked in purple, B-site cation in yellow, and X-sites anions marked in green and cyan.....	6
Figure 2	Depiction of an A-site centered perovskite unit cell. The A-site cation is marked in purple, B-site cation in yellow, and X-sites anions marked in green and cyan.....	6
Figure 3	Calculated tolerance factors for perovskite compounds where the A-site is occupied by methylammonium, the B-site is occupied by a divalent metal cation (Co-Ba), and the X-sites are composed strictly of oxygen, chlorine, bromine, or iodine.....	8
Figure 4	Calculated tolerance factors for hypothetical perovskites compounds where the A-site is occupied by methylammonium, the B-site is occupied by a trivalent metal cation (Ni-Pa), and the X-sites are a combination of oxygen and either chlorine, bromine, or iodine.	9
Figure 5	Calculated tolerance factors for hypothetical perovskites compounds where the A-site is occupied by methylammonium, the B-site is occupied by a trivalent metal cation (Ni-Pa), and the X-sites are a combination of oxygen and either chlorine, bromine, or iodine.	9
Figure 6	Illustrations of lines of contact within the perovskite unit cell. Left: x-axis octahedral contact length. Center: y-axis octahedral contact length. Right: z-axis octahedral contact length.	13
Figure 7	An illustration of the degree of tilting in a perovskite unit cell. The tilting associated with the atoms in the above 100 or 010 plane (they are identical here) is determined with respect to the B-site of the perovskite unit cell.	15
Figure 8	The A-centered 100 or 010 plane of hypothetical bismuth oxyhalide perovskite, wherein A-site cations (MA^{1+} or Cs^{1+}) are colored purple, B-site cations (Bi^{3+}) are colored yellow, X-site halides (Cl^{1-} , Br^{1-} , I^{1-}) are shown in green, and X-site oxygens (O^{2-}) are shown in blue.....	19
Figure 9	The A-centered 001 plane of hypothetical bismuth oxyhalide perovskite, wherein A-site cations (MA^{1+} or Cs^{1+}) are colored purple, B-site cations (Bi^{3+}) are colored yellow, X-site halides (Cl^{1-} , Br^{1-} , I^{1-}) are shown in green, and X-site oxygens (O^{2-}) are shown in blue.....	19

Figure 10	The A-centered 111 plane of hypothetical bismuth oxyhalide perovskite, wherein A-site cations (MA^{1+} or Cs^{1+}) are colored purple, B-site cations (Bi^{3+}) are colored yellow, X-site halides (Cl^{1-} , Br^{1-} , I^{1-}) are shown in green, and X-site oxygens (O^{2-}) are shown in blue.....	20
Figure 11	The B-centered 100 or 010 plane of hypothetical bismuth oxyhalide perovskite, wherein A-site cations (MA^{1+} or Cs^{1+}) are colored purple, B-site cations (Bi^{3+}) are colored yellow, X-site halides (Cl^{1-} , Br^{1-} , I^{1-}) are shown in green, and X-site oxygens (O^{2-}) are shown in blue.....	20
Figure 12	The B-centered 001 plane of hypothetical bismuth oxyhalide perovskite, wherein A-site cations (MA^{1+} or Cs^{1+}) are colored purple, B-site cations (Bi^{3+}) are colored yellow, X-site halides (Cl^{1-} , Br^{1-} , I^{1-}) are shown in green, and X-site oxygens (O^{2-}) are shown in blue.....	21
Figure 13	The B-centered 111 plane of hypothetical bismuth oxyhalide perovskite, wherein A-site cations (MA^{1+} or Cs^{1+}) are colored purple, B-site cations (Bi^{3+}) are colored yellow, X-site halides (Cl^{1-} , Br^{1-} , I^{1-}) are shown in green, and X-site oxygens (O^{2-}) are shown in blue.....	21
Figure 14	The XRD spectrum of bismuth oxychloride ($BiOCl$) reagent. Red peaks represent pattern matching to reported literature values used by the equipment software.....	27
Figure 15	The XRD spectrum of methylammonium chloride ($MACl$) reagent. Discrepancies between the pattern (black) and software matching (red) are attributed to the orientation of the crystal during analysis.	27
Figure 16	The XRD spectrum of cesium chloride ($CsCl$) reagent. This compound was not analyzed by XRD due to its hygroscopic nature, and was instead adopted from literature (cite).	28
Figure 17	Comparison of XRD spectra demonstrating the effects of halide substitution: (BLACK) Exp. 5: $BiOCl$ & $CsCl$ (1 Cs:1 Bi), $150^{\circ}C$, 3hrs. (BLUE) Exp. 7a: $BiOBr$ & $CsCl$ (1 Cs:1 Bi), $150^{\circ}C$, 3 hrs. (GREEN) Exp. 7b: $BiOI$ & $CsCl$ (1 Cs:1 Bi) $150^{\circ}C$, 3 hrs.....	29
Figure 18	Comparison of XRD spectra demonstrating the effects of halide substitution: (BLACK) Exp. 6: $BiOCl$ & $MACl$ (1 MA:1 Bi), $150^{\circ}C$, 3hrs. (BLUE) Exp. 8a: $BiOBr$ & $MACl$ (1 MA:1 Bi) $150^{\circ}C$, 3 hrs. (GREEN) Exp. 8b: $BiOI$ & $MACl$ (1 MA:1 Bi), $150^{\circ}C$, 3 hrs.	31

Figure 19	Comparison of XRD spectra demonstrating the effect of variable cation ratio at high temperatures: (BLACK) Exp. 12: BiOCl & CsCl, (1 Cs:1 Bi), 700°C, 22 hrs. (GREEN) Exp. 17: BiOCl & CsCl, (2 Cs:1 Bi), 700°C, 21.5 hrs. (BLUE) Exp. 18: BiOCl & CsCl, (3 Cs:1 Bi), 700°C, 21.5 hrs. (RED) Exp. 19: BiOCl & CsCl, (4 Cs:1 Bi), 700°C, 21.5 hrs.	33
Figure 20	Comparison of XRD spectra demonstrating the effect of heating duration: (BLACK) Exp 24: BiOCl & MACl (2.6 MA:1 Bi), 150°C, 1hrs. (RED) Exp 25a: BiOCl & MACl (2.6 MA:1 Bi) 150°C, 3 hrs. (BLUE) Exp 25b: BiOCl & MACl (2.6 MA:1 Bi), 150°C, 6 hrs. (GREEN) Exp 25c: BiOCl & MACl (2.6 MA:1 Bi), 150°C, 9 hrs.	35
Figure 21	Comparison of XRD spectra demonstrating the effects of heating duration: (RED) Exp 26a: BiOCl & MACl (2.6 MA:1 Bi) 150°C, 26.5 hrs. (BLACK) Exp 26b: BiOCl & MACl (2.6 MA:1 Bi), 150°C, 48.5 hrs.	37
Figure 22	Comparison of XRD spectra demonstrating the effects of variable cation ratio: (BLACK) BiOCl & MACl (1 MA:1 Bi), 150°C, 24hrs. (RED) BiOCl & MACl (2 MA:1 Bi) 150°C, 24 hrs. (BLUE) BiOCl & MACl (3 MA:1 Bi), 150°C, 24 hrs. (GREEN) BiOCl & MACl (4 MA:1 Bi), 150°C, 24 hrs.	39
Figure 23	A visualization of the $A_3B_2X_9$ unit cell, wherein the red atoms represent Bismuth B-site, grey represent halide atoms, and the blue-yellow molecules represent methylammonium or cesium. ⁴⁶	41
Figure 24	Exp. 5: BiOCl & CsCl (1 Cs:1 Bi), 150°C, 3hrs.	62
Figure 25	Exp. 7a: BiOBr & CsCl (1 Cs:1 Bi), 150°C, 3 hrs.	62
Figure 26	Exp. 7b: BiOI & CsCl (1 Cs:1 Bi) 150°C, 3 hrs.	63
Figure 27	Exp. 6: BiOCl & MACl (1 MA:1 Bi), 150°C, 3hrs.	63
Figure 28	Exp. 8a: BiOBr & MACl (1 MA:1 Bi) 150°C, 3 hrs.	64
Figure 29	Exp. 8b: BiOI & MACl (1 MA:1 Bi), 150°C, 3 hrs.	64
Figure 30	Exp. 12: BiOCl & CsCl, (1 Cs:1 Bi), 700°C, 22 hrs.	65
Figure 31	Exp. 17: BiOCl & CsCl, (2 Cs:1 Bi), 700°C, 21.5 hrs.	65
Figure 32	Exp. 18: BiOCl & CsCl, (3 Cs:1 Bi), 700°C, 21.5 hrs.	66

Figure 33	Exp. 19: BiOCl & CsCl, (4 Cs:1 Bi), 700°C, 21.5 hrs.....	66
Figure 34	Exp 24: BiOCl & MACl (2.6 MA:1 Bi), 150°C, 1hrs.....	67
Figure 35	Exp 25a: BiOCl & MACl (2.6 MA:1 Bi) 150°C, 3 hrs.....	67
Figure 36	Exp 25b: BiOCl & MACl (2.6 MA:1 Bi), 150°C, 6 hrs.....	68
Figure 37	Exp 25c: BiOCl & MACl (2.6 MA:1 Bi), 150°C, 9 hrs.....	68
Figure 38	Exp 26a: BiOCl & MACl (2.6 MA:1 Bi) 150°C, 26.5 hrs.....	69
Figure 39	Exp 26b: BiOCl & MACl (2.6 MA:1 Bi), 150°C, 48.5 hrs.....	69
Figure 40	Exp 27: BiOCl & MACl (1 MA:1 Bi), 150°C, 24hrs.....	70
Figure 41	Exp 28: BiOCl & MACl (2 MA:1 Bi) 150°C, 24 hrs.....	70
Figure 42	Exp 29: BiOCl & MACl (3 MA:1 Bi), 150°C, 24 hrs.....	71
Figure 43	Exp 30: BiOCl & MACl (4 MA:1 Bi), 150°C, 24 hrs.....	71

ABSTRACT

Despite notable advancements in light-harvesting technology, the costs associated with refining silicon to the purity necessary for solar cell applications have prevented this technology from being made available to the poorest and most in-need communities.¹ Over the past decade, research on a new light-harvesting structure, the hybrid organic-inorganic perovskite, has seen its single-junction power conversion efficiency jump from 3.8 % to over 22.1 % in little more than a decade.^{2,3} Meanwhile, silicon analog efficiencies have reached 26.3% after more than six decades of research and development.⁴

Compared to silicon solar cells, high-efficiency perovskites are easier to fabricate, cheaper to produce, less sensitive to chemical impurities, and highly tunable over wide ranges of band gap energies; making them suitable to a vast variety of applications for wavelengths up and down the electromagnetic spectrum.⁵ The most efficient perovskite structure published in the recent literature is methylammonium lead iodide (MAPbI₃).^{3,6} Despite its high performance, the acute toxicity and low stability of the lead moiety of this compound has challenged researchers to synthesize chemical variants that are not only safer and more stable, but also possess photoelectric efficiencies on par with that of MAPbI₃.⁷

The motivation for this work is to use the recent inception of perovskites in solar cell technology, along with bismuth- (lead's nontoxic neighbor)- to produce a solar cell from common, inexpensive, and safe materials. The substitution of lead with bismuth requires a change in the metal atom's valence state from +2 to +3, as well as the inclusion of a more easily-hybridized 6s lone pair.⁸ When hybridized, these electrons break the polyhedron backbone of the perovskite crystal, which could lead to

layered Aurivillius crystal phases instead of the desired perovskite structure.⁹ This work therefore aims to synthesize a bismuth perovskite compound in which the bismuth lone pair does not hybridize and the perovskite symmetry is preserved.

Chapter 1

INTRODUCTION

MOTIVATION

The thesis work described herein was designed to study hybridization of the bismuth 6s-lone pair of electrons, or lack thereof, in environments favorable to perovskite formation. Relying on previously successful dry-synthesis methods for perovskite formation,¹⁰ the intention of this paper was to synthesize a new family of perovskites that were less expensive than conventional silicon solar cells, less toxic, and significantly more stable than the best perovskite solar cells.⁷ Currently, the state of the art in the field of perovskite solar cell (PSC) research is a compound known as methylammonium lead iodide ((CH₃NH₃)PbI₃ or MAPbI₃ for short).¹¹ With a power conversion efficiency upwards of 22%, MAPbI₃ is one of the most efficient single-junction perovskite photocatalysts reported in literature.³ Unfortunately, due to the acute toxicity of the lead moiety and this compound's inability to survive extended periods of time under ambient conditions, researchers have been motivated to develop equally-as-efficient PSCs that last longer and pose fewer risks to people and the environment.⁷

Significant research has been conducted exploring the possibility of substituting out the lead cation in MAPbI₃ for another, less toxic element.¹² Tin has been studied in detail, given its homovalent electronic state and reduced toxicity, but perovskite compounds that successfully incorporate tin often fall victim to many of the same stability issues as the parent compound.¹³ Other elements, such as strontium

(Sr^{2+}),¹² Nickel (Ni^{2+}),¹⁴ and titanium (Ti^{2+})¹⁴ have also been explored as feasible alternatives, but none come close to rivaling the high single-junction power conversion efficiency of MAPbI_3 .

One less commonly taken approach to the substitution of lead involves swapping the toxic element out for one with a different valence number, in a process known as heterovalent substitution.¹⁵ While changing the number of electrons in the perovskite structure comes with its own complications—such as the necessity to minimize structural distortions and maintain charge neutrality¹⁶—the limited amount of literature on this subject provides us with the freedom to engineer novel perovskites and tailor their properties to fit our needs. Therefore, it would be valuable to the field of PSC research to set off into uncharted waters and explore the feasibility of new PSCs for photovoltaic applications.

The heterovalent element of interest here is bismuth, so chosen for its relatively low toxicity, inexpensive cost, and chemical proximity to lead in the periodic table, among other reasons.¹⁵ As mentioned previously, the valency of bismuth is one electron different from that of lead, complicating the substitution of bismuth into the MAPbI_3 framework. Bismuth's most common oxidation states are 3+ and 5+, whereas lead adopts a 2+ oxidation state in MAPbI_3 .¹⁷ Therefore, in order to construct a compound of neutral charge, it is also necessary to change other atoms in the compound to achieve zero charge overall. Options include swapping out the methylammonium cation, the halide anions, or a combination of the two until charge neutrality is achieved. While mixed halide compounds have been studied in detail as a means of tuning the band gap of existing PSCs to elicit the most ideal optoelectronic properties,¹⁸ almost no research has been conducted into mixed oxygen-halide PSCs,

so known as oxyhalide or chalcogenide perovskites. Several valid, charge-neutral compounds derived from the parent compound that also incorporate bismuth include $(\text{CH}_3\text{NH}_3)\text{BiOCl}_2$, $(\text{CH}_3\text{NH}_3)\text{BiOBr}_2$, $(\text{CH}_3\text{NH}_3)\text{BiOI}_2$, $(\text{CH}_3\text{NH}_3)\text{BiOClBr}$, $(\text{CH}_3\text{NH}_3)\text{BiOBrI}$, $(\text{CH}_3\text{NH}_3)\text{BiOClI}$, as well as the cesium analogs of these six compounds: CsBiOCl_2 , CsBiOBr_2 , CsBiOI_2 , CsBiOClBr , CsBiOBrI , CsBiOClI .

While mixed oxygen-halide compounds may not have yet been studied specifically related to perovskite systems, their promising performance in photovoltaic applications has already been well-established in literature.^{19,20} Bismuth oxyhalide compounds (BiOX , where X corresponds to the halides Cl, Br, and I) have demonstrated powerful light-mediated properties, including applications in pollutant degradation, water splitting, microbial deactivation and gas sensing.^{21,22} It would be interesting to see if the desirable photovoltaic properties of BiOX compounds carry over to proposed $(\text{CH}_3\text{NH}_3)\text{BiOX}_2$ and CsBiOX_2 compounds synthesized from them.

If maintaining charge neutrality is the first hurdle for bismuth PSCs, the second hurdle is the mitigation of structural distortions to the perovskite geometry. The functionality of PSCs is highly dependent upon the symmetry of the unit cell.²³ One of the most attractive electronic properties of MAPbI_3 , the optimal band gap, is intimately related to the structural crystal symmetry.²⁴ Reduction in the symmetry of the crystal results in an increased bandgap, making it harder for electrons to bridge the conduction and valence bands.²⁵ Therefore, significantly large degrees of tilting can result in the loss of the semiconducting properties of these perovskite compounds altogether.²³ Interestingly, MAPbI_3 itself possesses a sizable tilting of its octahedra.²⁶ This is due to the deviation of its tolerance factor from unity, which in turn is a consequence of the relative sizes of its constituent atoms. While the effect of

octahedral tilting is still poorly understood, it is known that the electronic properties of perovskite compounds deteriorate as their tolerance factors get further and further away from unity.²⁶ Therefore—in the hypothetical novel perovskite compounds envisioned in this work—it would be optimal to keep tilting distortions to a minimum.

One troubling reason that the octahedron would distort is due to hybridization of the heavy metal cation located at the center of the perovskite octahedra. While even lead possesses a 6s pair of electrons, the propensity of these electrons to hybridize, or dissociate from the nucleus and occupy physical space, is significantly less in lead than it is in bismuth. A hybridized lone pair of electrons would cause a significant distortion to the heavy metal's highly symmetric, six-fold coordination. The associated change in symmetry would lead to a change in space group and has been known to significantly alter the chemical properties of the compound. In some cases, hybridization has serendipitously lead to the development of new piezoelectric, ferroelectric, or optical properties.¹⁵ However, because we are motivated with the synthesis of photovoltaic compounds, it will be desirable to mitigate lone pair hybridization in favor of octahedral symmetry preservation.

In the work that follows, dry-synthesis methods reported in the literature will be applied to the synthesis of novel bismuth perovskites in an attempt to synthesize them and study their photovoltaic properties for solar cell applications. If the hypothetical compounds of interest can be synthesized, then it will show that bismuth hybridization does not occur, or does not occur to a sufficiently significant extent to deprive the resulting compound of its perovskite structure. If these compounds cannot be synthesized, one reason may be the hybridization of the 6s bismuth electrons, but

there are a variety of reasons that can and will be proposed for the lack of formation. These are discussed in Chapter 6 entitled, “Discussion.”

PEROVSKITE UNIT CELL

A perovskite is a crystal structure made up of at least three different atoms, generalized as “A”, “B”, and “X.” The arrangement of these atoms in the cubic unit cell of a three-dimensional crystal can be represented in two ways, with an A-site or B-site centered unit cell. Both representations are illustrated below in Figures 1 and 2. In an extended system, A-sites are populated by cationic species possessing ionic radii greater than that of the B-site atom, which is also a cation. The X-site atoms are anions, typically halides (such as chlorine, bromine, or iodine) or chalcogens (such as oxygen), but never both. The X-sites occupy an octahedral geometry around the B-site cation, while the A-sites occupy the interstices between octahedra.²⁷ A-site cations are coordinated to twelve X-site anions, B-site cations are coordinated to six X-site anions, and X-site anions are coordinated to two B-site cations. Many variations of perovskites exist, including two-dimensional,¹¹ one-dimensional,²⁸ double,²⁹ and layered³⁰ (including Ruddleson-Popper,³¹ Aurivillius,³² Dion-Jacobson phases³³) to name a few.

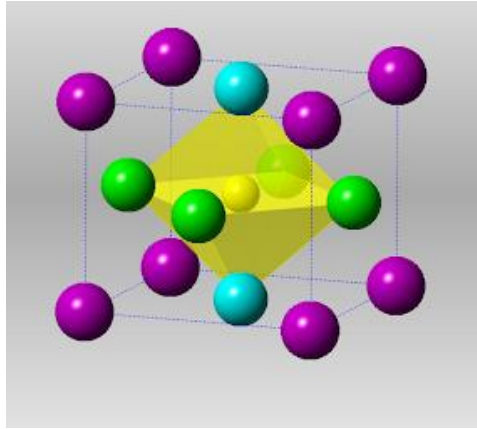


Figure 1 Depiction of an B-site centered perovskite unit cell. The A-site cation is marked in purple, B-site cation in yellow, and X-sites anions marked in green and cyan.

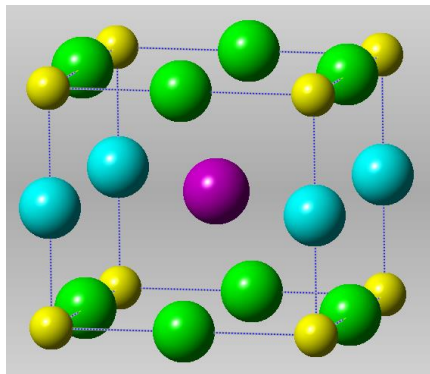


Figure 2 Depiction of an A-site centered perovskite unit cell. The A-site cation is marked in purple, B-site cation in yellow, and X-sites anions marked in green and cyan.

TOLERANCE FACTOR

Many different combinations of atoms can be made to adapt the perovskite crystal structure given that they satisfy certain criteria. For charge neutral compounds satisfying the formula ABX_3 , where the ionic radius of the A-site cation is greater than that of the B-site, the Goldschmidt tolerance factor is frequently cited as the most

pertinent metric in predicting whether or not the formation of the perovskite structure is possible.^{26,34,35} By taking the relative differences of ionic radii into account, the tolerance factor is used to indicate the degree to which the octahedral geometry of the perovskite structure can be achieved given the radii of the atoms involved.²⁶ The tolerance factor is typically defined as the scaled ratio of the sum of the A- and X-site ions over the sum of the B- and X-site ions, multiplied by the squared root of two,³⁴ depicted below as Equation 1.

$$t = \frac{r_A + r_X}{\sqrt{2}(r_B + r_X)} \quad (1)$$

Typically, perovskites are made up on anions that are all the same chemical species, such as all oxygen, all chlorine, etc. However, due to the novelty of mixing anions in the hypothetical compounds being investigated in this thesis, the tolerance factor will have to be adjusted slightly to take into account the mixed oxygen-halide X-sites. Doing so will result in a tolerance factor that more accurately reflects the geometric constraints of the proposed compounds of interest.

The tolerance factor can be rectified by recognizing that the A-site/X-site distance computed in the numerator of the tolerance factor is actually an A-site/O-site distance. This relatively minor change is reflected in the following, corrected equation, Equation 2.

$$t = \frac{r_A + r_O}{\sqrt{2}(r_B + r_X)} \quad (2)$$

While a tolerance factor of unity corresponds to the ideal cubic perovskite, many other stable perovskite structures have a tolerance factor in the range of 0.85 to 1.02.²⁶ Tolerance factors less than one are often associated with octahedral tilting

within the unit cell, as is the case with the well-known photovoltaic perovskite, methylammonium lead iodide (MAPbI₃).²⁴ This tilting can have interesting consequences on the chemical and electronic properties of the bulk crystal, such as piezoelectricity, ferroelectricity, and the manifestation of nonlinear optical properties.²⁶

Armed with a corrected tolerance factor equation, it is now possible to screen potential perovskite materials for their structural feasibility based off of their crystal radii. Figures 4 and 5 below illustrate the tolerance factors predicted from on wide range of heterovalent B-site alternatives.

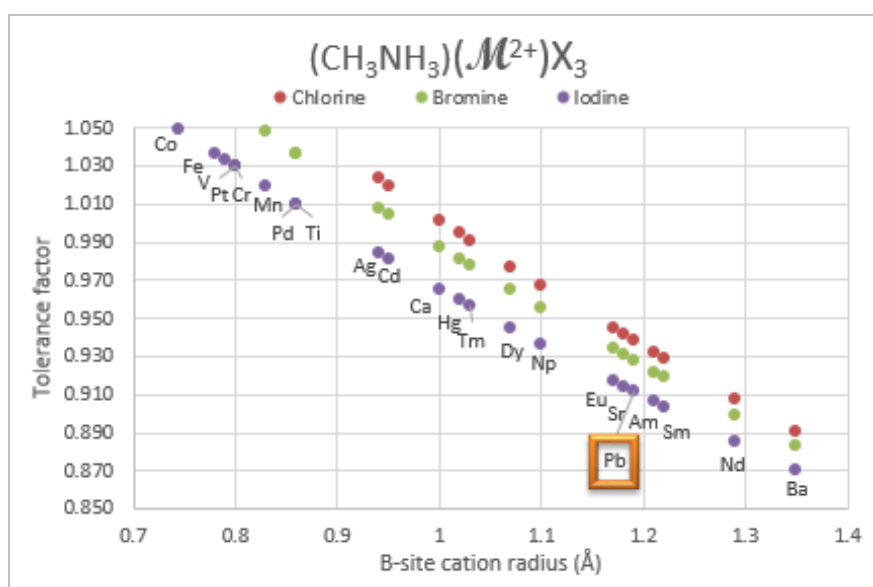


Figure 3 Calculated tolerance factors for perovskite compounds where the A-site is occupied by methylammonium, the B-site is occupied by a divalent metal cation (Co-Ba), and the X-sites are composed strictly of oxygen, chlorine, bromine, or iodine.

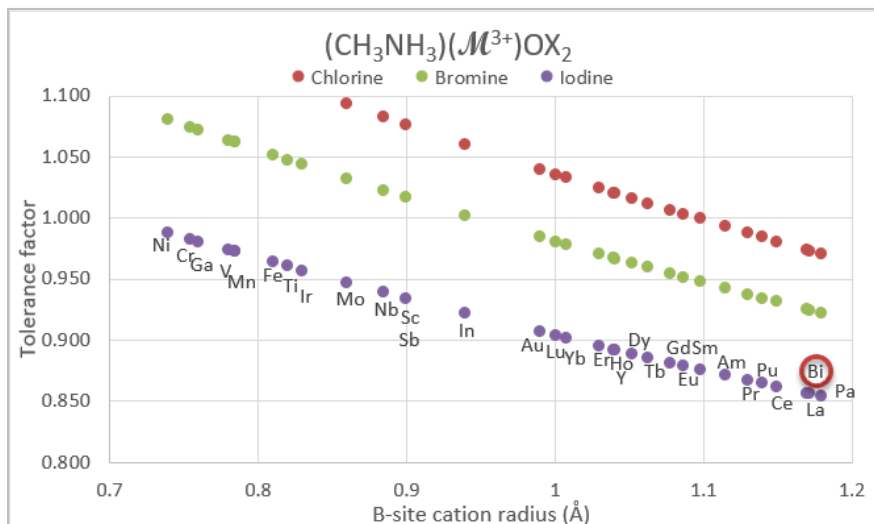


Figure 4 Calculated tolerance factors for hypothetical perovskites compounds where the A-site is occupied by methylammonium, the B-site is occupied by a trivalent metal cation (Ni-Pa), and the X-sites are a combination of oxygen and either chlorine, bromine, or iodine.

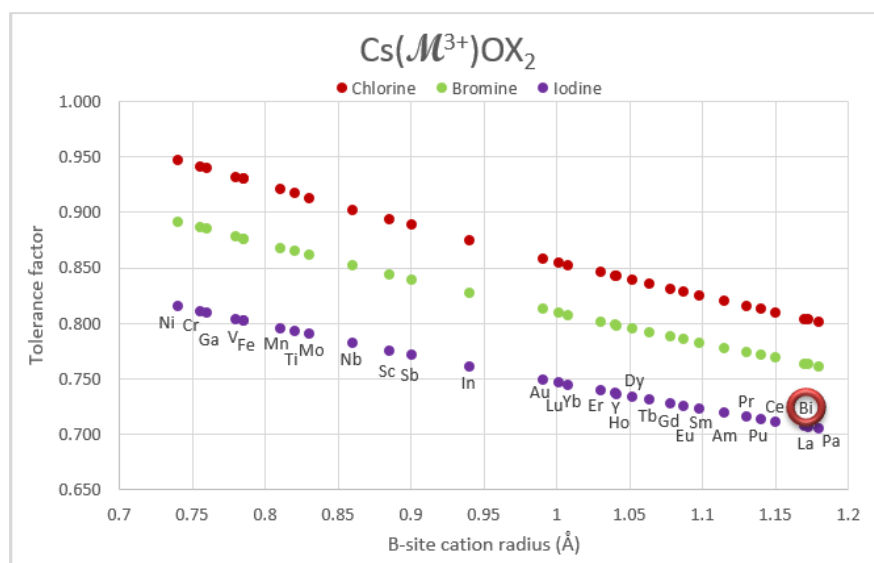


Figure 5 Calculated tolerance factors for hypothetical perovskites compounds where the A-site is occupied by methylammonium, the B-site is occupied by a trivalent metal cation (Ni-Pa), and the X-sites are a combination of oxygen and either chlorine, bromine, or iodine.

As can be deduced from Figure 3, MAPbI₃ (a hugely successful photovoltaic perovskite compound^{11,36}), possesses a tolerance factor of 0.912. As it turns out, many photoactive perovskite compounds actually possess tolerance factors less than unity, wherein octahedral tilting is known to occur and deviation from the “ideal” perovskite structure is observed.³⁷ Remembering that perovskite formation is most favorable for compounds with tolerance factors between 0.85 and 1.02,²⁶ Figure 4 shows that MABiOI₂ would likely not result in the desired perovskite structure, while the chlorine and bromine analogs would. But because MABiOCl₂ and MABiOBr₂ have tolerance factors of 0.974 and 0.925, respectively, it is likely that the octahedra within these compounds will be tilted, should they form at all.

The second family of hypothetical compounds that was evaluated was CsBiOX₂. As can be deduced from Figure 5, there is no CsBiOX₂ compound for which the tolerance factor is expected to be greater than 0.85. From this first principles approach, it would appear as though perovskite formation will not be possible in this hypothetical family of compounds. However, as a means of verifying the accuracy of the tolerance factor, experiments designed in Chapter 3, “Experimental Methods,” were conducted in an attempt to synthesize these cesium bismuth oxyhalide compounds anyway to see what structures would form instead.

Note that, due to the inability of the tolerance factor equation to take three anionic species into account, it was not possible to calculate the tolerance factor for mixed halide bismuth oxyhalide species, such as MABiOClBr. As such, it was assumed that the tolerance factors for these compounds were taken to lie somewhere between the pure-halide versions of these compounds (between the tolerance factors of such compounds as MABiOCl₂ and MABiOBr₂, for example).

LONE PAIR ELECTRON HYBRIDIZATION

In crystalline perovskite structures, hybridization of the 6s-electron orbitals results in the formation of a stereochemically active lobe of electron density, termed an “inert lone pair.”³⁸ This pair of electrons makes up a near-spherical hybridized lobe that takes up a region of space approximately equal to the size of an oxide or fluoride anion³⁹ (about 1.34 angstroms).⁴⁰ Unlike these anions however, the lone pair are more closely localized to the B-site cation they belong to than the coordinated anions located at the vertices of the octahedron.³⁹ The highly localized pair of electrons cause a displacement distortion that shifts the B-site cation away from the true center of the octahedron.³⁹ The repulsive forces of the hybridized electron lobe push the other anions away, breaking the octahedral and unit cell symmetry, completely distorting the structure of the hybridized compound.⁴¹ When this occurs in photovoltaic perovskite compounds, the desirable light-active properties disappear and the compound can no longer be used as a light-absorbing agent in solar harvesting technology.⁴² That being said, it will be essential to understand the underlying mechanisms of bismuth hybridization if we are to have the best chances of producing stable, unhybridized perovskite compounds.

HYPOTHESIS

Having developed this basic understanding of perovskites, their photovoltaic properties, and their structures, it is now possible to formulate an informed statement designed to probe the limits of current knowledge and learn more about photoactive perovskite compounds. So being, it is the formal hypothesis of this study to posit that: if previously successful dry-synthesis methods are applied to the synthesis of novel bismuth oxyhalide compounds, then these compounds will indeed be successfully

synthesized. Observation of the desired perovskite compounds is the only definitive means of confirming this hypothesis. Lack thereof could be due to any number of reasons, but those most relevant to this study involve lone-pair hybridization as it relates to the presence of the bismuth cation.⁸

Chapter 2

PRECALCULATIONS

FIRST-PRINCIPLES LATTICE CONSTANT PREDICTIONS

Due to the hypothetical nature of the proposed perovskite compounds, empirical lattice constants do not exist, as they have never before been reported in the literature. Instead, a first-principles application of geometry to the atoms in the perovskite unit cell was used to estimate the lattice cell dimensions.

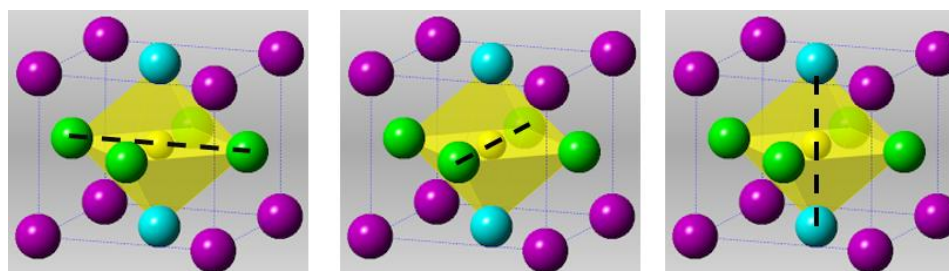


Figure 6 Illustrations of lines of contact within the perovskite unit cell. Left: x-axis octahedral contact length. Center: y-axis octahedral contact length. Right: z-axis octahedral contact length.

Line of Contact (MA ¹⁺ A-site)	O-Bi-O	Cl-Bi-Cl	Br-Bi-Br	I-Bi-I
Length (Å)	4.760	5.680	5.980	6.460

Table 1 Calculation of the predicted dimension length derived from the length of each contact axis of the hypothetical methylammonium bismuth oxyhalide octahedra.

Lattice Parameter Compound	“a” (Å)	“b” (Å)	“c” (Å)
(CH ₃ NH ₃)BiOCl ₂	5.680	5.680	4.760
(CH ₃ NH ₃)BiOBr ₂	5.980	5.980	4.760
(CH ₃ NH ₃)BiOI ₂	6.460	6.460	4.760
(CH ₃ NH ₃)BiOClBr	5.680	5.980	4.760
(CH ₃ NH ₃)BiOBrI	5.980	6.460	4.760
(CH ₃ NH ₃)BiOClI	5.680	6.460	4.760

Table 2 A summarization of the predicted lattice parameters for the hypothetical compounds of interest. Green, red, purple, and blue shading refers to the oxygen, chlorine, bromine, and iodine contributions, respectively.

As is evident from Tables 1 and 2 above, it is possible to predict the crystal system of the methylammonium bismuth oxyhalide compounds based off of their estimated lattice constants. Edge lengths were estimated as the sum of the crystal radii of the ions constituting the octahedron. For example, the horizontal lattice constant of a bismuth oxychlorine compound was calculated as the sum of two oxygen and one bismuth crystal radii. The pure-halide compounds (MABiOCl₂, MABiOBr₂, MABiOI₂) are likely to be tetrahedral while the mixed halide compounds (MABiOClBr, MABiOBrI, MABiOClI), will probably be orthorhombic, should they be observed. Given that all of the proposed compounds have X-sites that contain anions of different sizes, a cubic perovskite is not expected for any of the compounds.

Note that the inherent assumption in the predictions of the above lattice parameters is that there is no tilting in the perovskite octahedron, despite the fact that some electronic properties of these structures are rooted in their characteristic tilting distortions. Therefore, in order to make this calculation inclusive of such tilting distortions, it is worthwhile to develop expressions founded in the perovskite

geometry that can relate the degree of tilting of the perovskite octahedron to the value of the lattice constants.

Trigonometric relations were used to relate the degree of tilting in the x-, y-, and z-directions to the unit cell lattice constants: “a,” “b,” and “c.” Referencing the degree of tilt to the B-site of the unit cell, the degree of tilt in a given direction can be broken down into its x- and y-components. The lattice parameter “a” was only affected by x-dimensional tilting and “b” was only affected by y-dimensional tilting, while “c” was a function of both the x- and y-dimensional tilting. The anion-to-anion distance of the perovskite octahedron in either the x- or y-plane, multiplied by the cosine of the degree of tilt in that plane gives the value of the tilted “a” or “b” lattice parameter, respectively. The change in the z-dimensional “c” parameter is the anion-to-anion length of the perovskite octahedron in the z-plane multiplied by both cosines for the angle of tilt in the x- and y-dimensions.

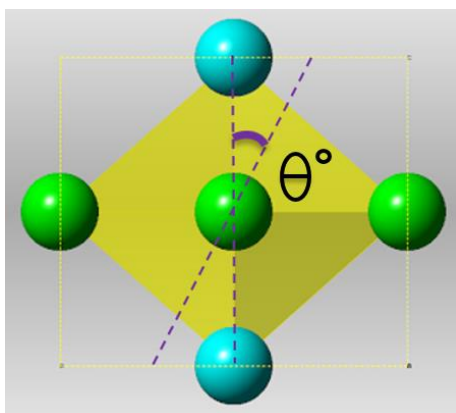


Figure 7 An illustration of the degree of tilting in a perovskite unit cell. The tilting associated with the atoms in the above 100 or 010 plane (they are identical here) is determined with respect to the B-site of the perovskite unit cell.

General expressions relating the degree of tilt in the axial dimensions of the octahedron to the distorted lattice parameters were derived (see Equations 3 to 5 below). As an example, values for the lattice parameters of methylammonium bismuth oxychloride ((CH₃NH₃)BiOCl₂) that took tilting into account were tabulated at various tilt angles and reported below in Table 3.

$$a' = (a) \cos(\theta) \quad (3)$$

$$b' = (b) \cos(\varphi) \quad (4)$$

$$c' = (c) \cos(\theta) \cos(\varphi) \quad (5)$$

where a', a, θ , and φ are defined as the distorted and undistorted lattice parameters, the x-dimensional angle of tilt, and the y-dimensional angle of tilt, respectively.

(CH₃NH₃)BiOCl₂

x-tilt (θ°) y-tilt (φ°)	0° (Å)	15° (Å)	30° (Å)	45° (Å)
0° (Å)	a=5.680 b=5.680 c=4.760	a=5.486 b=5.680 c=4.598	A=4.919 b=5.680 c=4.122	a=4.016 b=5.680 c=3.366
15° (Å)	a=5.680 b=5.486 c=4.598	a=5.486 b=5.486 c=4.441	a=4.919 b=5.486 c=3.982	a=4.016 b=5.486 c=3.251
30° (Å)	a=5.680 b=4.919 c=4.122	a=5.486 b=4.919 c=3.982	a=4.919 b=4.919 c=3.092	a=4.016 b=4.919 c=2.915
45° (Å)	a=5.680 b=4.016 c=3.366	a=5.486 b=4.016 c=3.251	a=4.919 b=4.016 c=2.915	a=4.016 b=4.016 c=2.380

Table 3 Lattice parameters calculated for arbitrary angles of tilt in the specified perovskite octahedron. The origin of the tilting angle was taken to be the B-site of the unit cell.

With the ability to estimate the lattice constants for the hypothetical compounds discussed here, it is also possible to predict the XRD peak angles associated with each of the compounds of interest. Table 4 below includes a collection of the possible peaks that could be observed for the family of hypothetical methylammonium bismuth oxyhalide compounds. Notice that the determination of the d-spacing value assumes that the crystal system predicted from the lattice constants (i.e. tetragonal or orthorhombic) is indeed the crystal system of the pure-halide or mixed halide compound, respectively.

The following table summarizes the peak angles that one should expect to observe for the hypothetical compounds posited in this thesis based on the lattice constants calculated previously in this chapter. Hypothetical d-spacing were calculated for each of the compounds assuming orthorhombic crystal symmetry (Equation 6 below). With the d-spacings known, Bragg's law was used to back out the expected peak angles of these compounds (Equation 7). While not all of the peaks calculated from this method are always observed, assumptions were made as to the symmetry group of the hypothetical compounds, such that forbidden reflections need be removed. Table 4 assumes symmetry groups I4/mcm and Pnma for the tetragonal and orthorhombic crystal symmetries, respectively.

$$d = \left(\frac{h^2}{a^2} + \frac{k^2}{b^2} + \frac{l^2}{c^2} \right)^{0.5} \quad (6)$$

$$n\lambda = 2d * \sin(\theta) \quad (7)$$

XRD SPECTRA PREDICTIONS

h	k	l	2θ (Tetragonal)			2θ (Orthorhombic)		
			MABiOCl ₂	MABiOBr ₂	MABiOI ₂	MABiOClBr	MABiOClI	MABiOBrI
1	0	0	15.589	14.802	13.697	15.589	15.589	14.802
0	1	0	15.589	14.802	13.697	14.802	13.697	13.697
0	0	1	18.626	18.626	18.626	18.626	18.626	18.626
1	1	0	22.115	20.992	19.417	21.560	20.807	20.219
0	1	1	24.378	23.874	23.193	23.874	23.193	23.193
1	0	1	24.378	23.874	23.193	24.378	24.378	23.874
1	1	1	29.066	28.206	27.032	28.639	28.066	27.625
2	0	0	31.475	29.858	27.594	31.475	31.475	29.858
0	2	0	31.475	29.858	27.594	29.858	27.594	27.594
1	2	0	35.305	33.481	30.928	33.852	31.846	31.453
2	1	0	35.305	33.481	30.928	34.947	34.469	32.984
0	2	1	36.823	35.424	33.501	35.424	33.501	33.501
2	0	1	36.823	35.424	33.501	36.823	36.823	35.424
0	0	2	37.768	37.768	37.768	37.768	37.768	37.768
1	2	1	40.208	38.584	36.347	38.913	37.147	36.804
2	1	1	40.208	38.584	36.347	39.888	39.461	38.145
0	1	2	41.087	40.772	40.354	40.772	40.354	40.354
1	0	2	41.087	40.772	40.354	41.087	41.087	40.772
1	1	2	44.199	43.604	42.809	43.902	43.508	43.208
2	2	0	45.111	42.734	39.421	43.935	42.344	41.105
3	0	0	48.014	45.466	41.921	48.014	48.014	45.466
0	3	0	48.014	45.466	41.921	45.466	41.921	41.921
2	2	1	49.205	46.989	43.935	48.107	46.627	45.482
0	2	2	49.957	48.871	47.410	48.871	47.410	47.410
2	0	2	49.957	48.871	47.410	49.957	49.957	48.871
1	3	0	50.790	48.076	44.305	48.352	44.986	44.693

Table 4 Peak angles for six hypothetical bismuth oxyhalide compounds were calculated from the predicted lattice constants found for perovskites containing the respective atom, assuming no tilting of the octahedron.

HYPOTHETICAL UNIT CELL

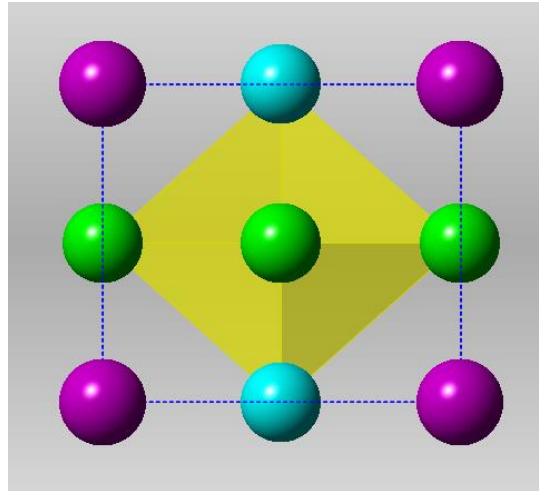


Figure 8 The A-centered 100 or 010 plane of hypothetical bismuth oxyhalide perovskite, wherein A-site cations (MA^{1+} or Cs^{1+}) are colored purple, B-site cations (Bi^{3+}) are colored yellow, X-site halides (Cl^{1-} , Br^{1-} , I^{1-}) are shown in green, and X-site oxygens (O^{2-}) are shown in blue.

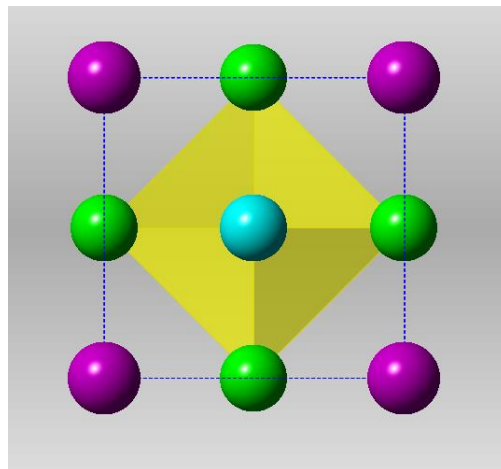


Figure 9 The A-centered 001 plane of hypothetical bismuth oxyhalide perovskite, wherein A-site cations (MA^{1+} or Cs^{1+}) are colored purple, B-site cations (Bi^{3+}) are colored yellow, X-site halides (Cl^{1-} , Br^{1-} , I^{1-}) are shown in green, and X-site oxygens (O^{2-}) are shown in blue.

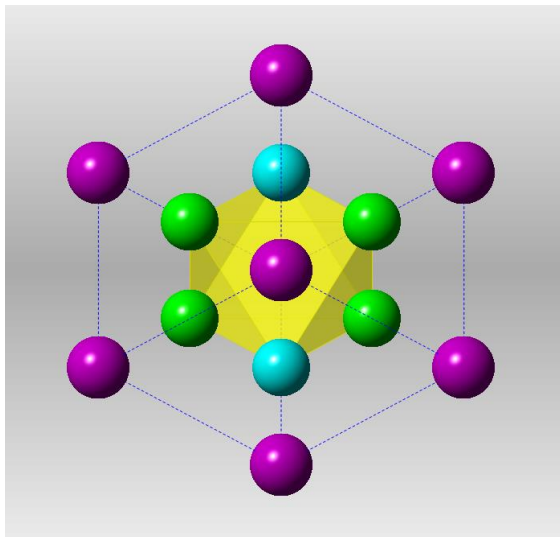


Figure 10 The A-centered 111 plane of hypothetical bismuth oxyhalide perovskite, wherein A-site cations (MA^{1+} or Cs^{1+}) are colored purple, B-site cations (Bi^{3+}) are colored yellow, X-site halides (Cl^{1-} , Br^{1-} , I^{1-}) are shown in green, and X-site oxygens (O^{2-}) are shown in blue.

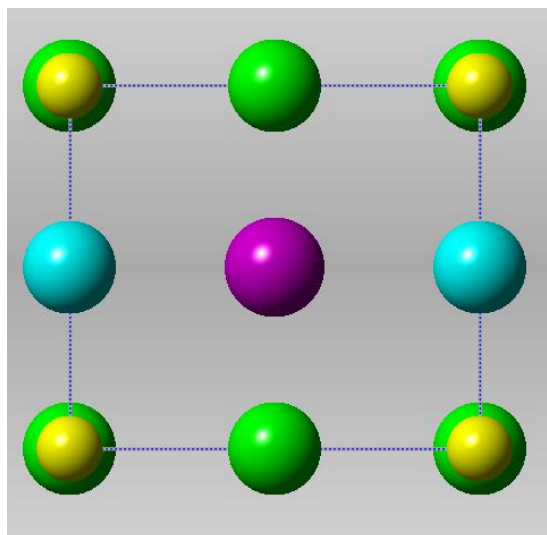


Figure 11 The B-centered 100 or 010 plane of hypothetical bismuth oxyhalide perovskite, wherein A-site cations (MA^{1+} or Cs^{1+}) are colored purple, B-site cations (Bi^{3+}) are colored yellow, X-site halides (Cl^{1-} , Br^{1-} , I^{1-}) are shown in green, and X-site oxygens (O^{2-}) are shown in blue.

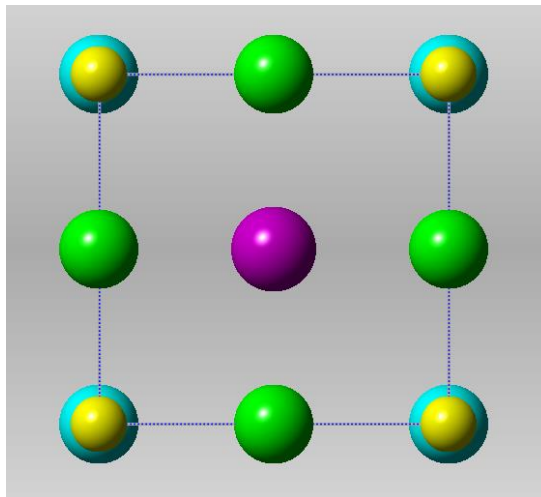


Figure 12 The B-centered 001 plane of hypothetical bismuth oxyhalide perovskite, wherein A-site cations (MA^{1+} or Cs^{1+}) are colored purple, B-site cations (Bi^{3+}) are colored yellow, X-site halides (Cl^{1-} , Br^{1-} , I^{1-}) are shown in green, and X-site oxygens (O^{2-}) are shown in blue.

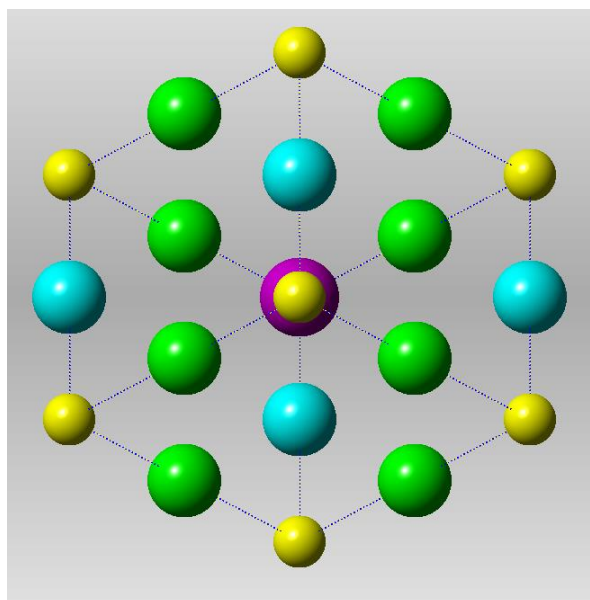


Figure 13 The B-centered 111 plane of hypothetical bismuth oxyhalide perovskite, wherein A-site cations (MA^{1+} or Cs^{1+}) are colored purple, B-site cations (Bi^{3+}) are colored yellow, X-site halides (Cl^{1-} , Br^{1-} , I^{1-}) are shown in green, and X-site oxygens (O^{2-}) are shown in blue.

Chapter 3

EXPERIMENTAL METHODS

REAGENTS

A one-kilogram container of bismuth nitrate pentahydrate, $(\text{Bi}(\text{NO}_3)_3 \cdot 5(\text{H}_2\text{O}))$, was purchased from Alfa Aesar at a purity of 98%, CAS-No. 10035-06-0. Two and a half liters of concentrated hydrochloric acid stored in the acids cabinet was purchased from Fischer Scientific, CAS-No. 7647-01-0. Methylammonium chloride (MACl) was purchased specifically for these experiments from EMD Millipore Corporation with a purity of 99.0%, CAS-No. 593-51-1. Cesium chloride (CsCl) was distributed by Aldrich Chemical Company at 99.9995% purity, sealed with electrical tape to prevent hygroscopic absorption of water, CAS-No. 7647-17-8. Deionized water was obtained from the laboratory tap.

BISMUTH OXYCHLORIDE SYNTHESIS

Bismuth oxychloride (BiOCl) was synthesized by allowing 10 grams of bismuth nitrate pentahydrate ($\text{Bi}(\text{NO}_3)_3 \cdot 5(\text{H}_2\text{O})$) to completely dissolve in 10 mL of concentrated hydrochloric acid (HCl). Once dissolved, 50 milliliters of deionized water was added to the clear solution, resulting in the formation of a white precipitate. The solution was then centrifuged at 1000 rpm for 10 minutes to condense the precipitate into a pellet. The supernatant was removed before immersing the pellet in deionized water and shaking until the powder solid was completely resuspended in

deionized water. The solution was again centrifuged at 1000 rpm for 10 minutes. Once again, the supernatant was removed. Washing with deionized water was repeated twice more. Then, the solid pellet removed placed on a watch glasses to dry in the fume hood. The dried solid was characterized by X-Ray Powder Diffraction to match the known spectrum for bismuth oxychloride. Bismuth oxybromide and bismuth oxyiodide were made by previous principle investigators of the Buttrey lab.

CESIUM CHLORIDE HANDLING

Due to the highly hygroscopic nature of cesium chloride, a glove bag was used to weigh the reagent mass for experiments involving cesium chloride. The bag was inflated half-way with nitrogen gas and deflated three times to minimize the presence of water vapor within the bag. A weigh balance was placed inside of the glove bag and holes for wires were sealed tightly with tape.

SAMPLE SYNTHESIS

Prelab calculations were carried out to determine the masses that corresponded to molar ratios of the two chemicals being reacted in any given experiment, typically 1:1 but as much as 4:1 in some cases. The desired quantities of reactants were weighed separately on a mass balance before being ground by hand with a mortar and pestle for approximately one minute. The samples were then placed into an alumina crucible and placed in a preheated oven or furnace—whichever was could achieve the required

heating temperature. Once heated, the crucibles were removed with tongs, allowed to cool naturally to room temperature, and placed into glass vials for storage before being analyzed by X-ray Powder Diffraction.

CRUCIBLE CLEANING

Alumina crucibles were used to hold the samples while being heated in the laboratory oven. In order to clean the crucibles between experiments and ensure no residual carry over of chemical contaminants, the crucibles were washed with soap and warm water. Any powders that adhered stubbornly to the bottom of the crucibles were removed by soaking in warm water overnight.

SAMPLE CHARACTERIZATION

After heating, cooled samples were analyzed by X-ray Powder Diffraction using the Rigaku XRD instrument in the Advanced Materials Characterization lab. Samples were analyzed using X-rays of 1.54060 Å wavelength, shutter speeds of 3 seconds, and a range of 2θ diffraction angles spanning 5° - 60° in 0.02° increments. A single run commonly required 2.5 hours to achieve an acceptable level of signal-to-noise distinction.

EXPERIMENTAL CONDITIONS

Experimental attempts to synthesize the hypothetical compounds of interest were conducted through the solid-state reaction of a salt (MACl or CsCl) and a bismuth oxyhalide compound (BiOCl, BiOBr, or BiOI). The following reaction conditions were tested for perovskite formation.

Rxn	MA (g)	CsCl (g)	BiOCl (g)	BiOBr (g)	BiOI (g)	Molar Ratio (A/B)	Temperature (°C)	Duration (hrs.)
4	-	0.647	1.000	-	-	1:1	150	3
5	-	0.136	0.506	-	-	1:1	150	3
6	0.136	-	0.506	-	-	1:1	150	3
7a	-	0.188	-	0.500	-	1:1	150	3
7b	-	0.239	-	-	0.500	1:1	150	3
8a	0.096	-	-	0.505	-	1:1	150	3
8b	0.075	-	-	-	0.510	1:1	150	3
9	-	0.332	0.508	-	-	1:1	200	112
10	-	0.331	0.509	-	-	1:1	509	16.5
11*	-	0.331	-	0.505	-	1:1	500, 600, 600	28, 2, 4
12*	-	0.333	0.508	-	-	1:1	700	22
13*	-	0.329	0.508	-	-	1:1	800	17.5
14	-	0.330	0.133	-	-	4:1	800	17.5
15*	-	0.330	0.174	-	-	3:1	600	71
16*	-	0.330	0.256	-	-	2:1	700	24
17	-	0.328	0.256	-	-	2:1	700	21.5
18	-	0.328	0.172	-	-	3:1	700	21.5
19	-	0.328	0.171	-	-	4:1	700	21.5
20	0.048	-	0.158	-	-	1:1	150	24
21	0.048	-	0.158	-	-	1:1	150	48
22	0.084	-	0.157	-	-	2:1	150	24
23	0.122	-	0.155	-	-	3:1	150	24
24	0.114	-	0.164	-	-	2.6:1	150	1
25a	0.114	-	0.163	-	-	2.6:1	150	3
25b	0.115	-	0.163	-	-	2.6:1	150	6
25c	0.116	-	0.162	-	-	2.6:1	150	9
25d	0.116	-	0.165	-	-	2.6:1	150	12
26a	0.114	-	0.163	-	-	2.6:1	150	26.5

26b	0.114	-	0.163	-	-	2.6:1	150	48.5
27	0.052	-	0.200	-	-	1:1	150	24
28	0.052	-	0.100	-	-	2:1	150	24
29	0.078	-	0.100	-	-	3:1	150	24
30	0.104	-	0.100	-	-	4:1	150	24
31	0.052	-	0.200	-	-	1:1	150	48
32	0.052	-	0.100	-	-	2:1	150	48

Table 5 Summary of pertinent experimental factors in laboratory attempts to synthesize the perovskite compounds of interest. (*)-marked experiments are meant to indicate that silicon standard was added to check the calibration of the XRD instrument. Greyed out experiments were not analyzed due to contamination or believed to not be insightful.

Chapter 4

REAGENT XRD PATTERNS

BISMUTH OXYCHLORIDE

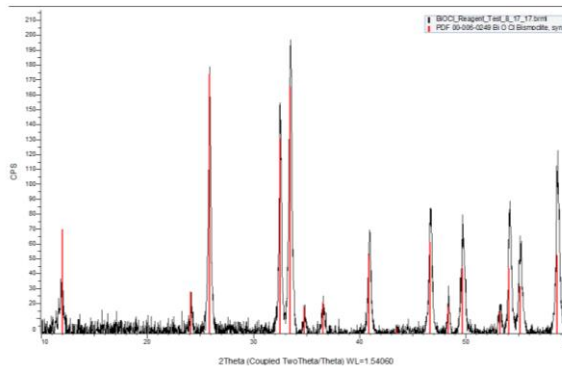


Figure 14 The XRD spectrum of bismuth oxychloride (BiOCl) reagent. Red peaks represent pattern matching to reported literature values used by the equipment software.

METHYLAMMONIUM CHLORIDE

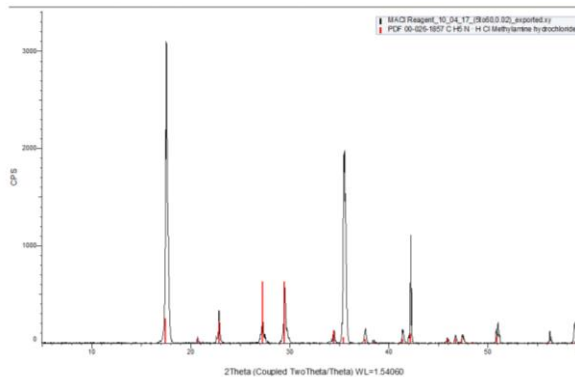


Figure 15 The XRD spectrum of methylammonium chloride (MACl) reagent. Discrepancies between the pattern (**black**) and software matching (**red**) are attributed to the orientation of the crystal during analysis.

The above spectra were analyzed by Rigaku X-ray Powder Diffraction software to ascertain the location and intensity of peaks common to the BiOCl and (CH₃NH₃)Cl reagents so that they can be identified in experiments wherein unreacted BiOCl or (CH₃NH₃)Cl is present. The XRD software comes with a crystal identification package that is meant to facilitate this identification.

CESIUM CHLORIDE

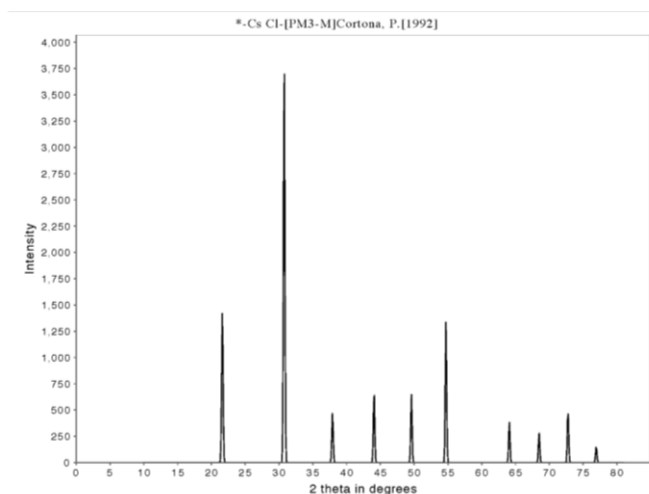


Figure 16 The XRD spectrum of cesium chloride (CsCl) reagent. This compound was not analyzed by XRD due to its hygroscopic nature, and was instead adopted from literature (cite).

The above figure depicts the X-ray Powder Diffraction pattern of the reagent Cesium Chloride (CsCl). Given the highly hygroscopic nature of this compound and the lengthy run time necessary to obtain reasonable signal-to-noise ratios, the above pattern was not analyzed by XRD but rather reprinted from a reputable source.⁴³

Chapter 5

PRODUCT XRD PATTERNS

EXPERIMENTS 5, 7a, & 7b

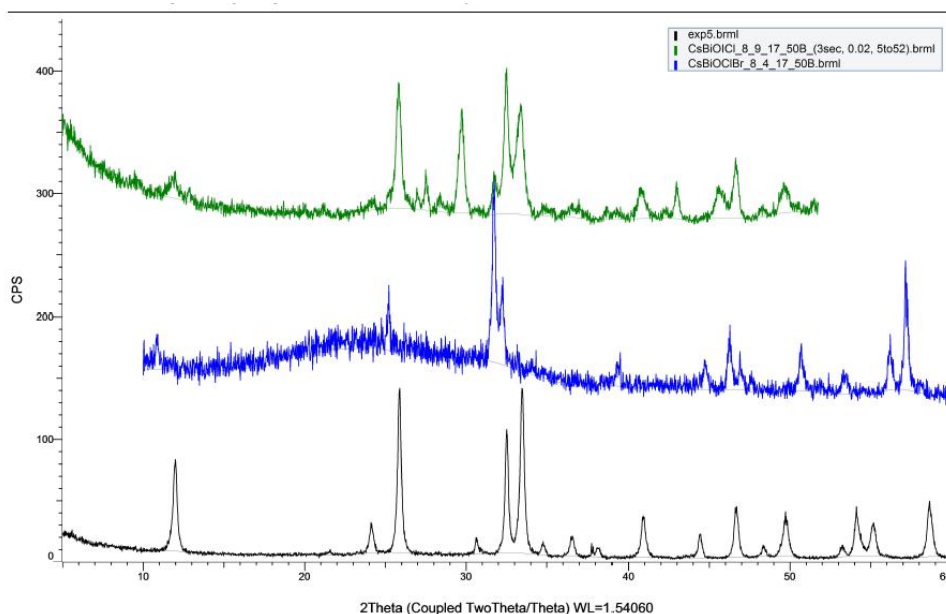


Figure 17 Comparison of XRD spectra demonstrating the effects of halide substitution:

(BLACK) Exp. 5: BiOCl & CsCl (1 Cs:1 Bi), 150°C, 3hrs.

(BLUE) Exp. 7a: BiOBr & CsCl (1 Cs:1 Bi), 150°C, 3 hrs.

(GREEN) Exp. 7b: BiOI & CsCl (1 Cs:1 Bi) 150°C, 3 hrs.

The above three spectra illustrate the different x-ray powder diffraction patterns for the reaction products of cesium chloride with each of the three bismuth oxyhalides. The pattern matching software analyzing the BiOCl & CsCl reaction found a 96% match for Bismoclite (aka. BiOCl), indicating unreacted BiOCl reagent in the product (see Appendix B). While many of the peaks of this pattern corresponded

to characteristic peaks for BiOCl, five low-intensity peaks were also observed, corresponding to the diffraction pattern of CsCl. Therefore, unreacted cesium chloride can also be observed in the sample, with no evidence of reaction.

In the BiOBr & CsCl reaction, there was an 89% match for unreacted BiOBr (see Appendix B). No other peaks were discerned, indicating that there was no evidence whatsoever of the cesium atoms in the XRD sample. It was postulated that the cesium moiety had vaporized away during the heating process.

The BiOI & CsCl reaction sample showed signs of unreacted BiOI and CsCl, but this time, a new phase was identified with 54% reliability: cesium nonaiododibismuthate(III) ($\text{Cs}_3\text{Bi}_2\text{I}_9$). The space group of this compound is P63/mmc in a hexagonal crystal system. The “a” lattice constant measures 8.4116 Å, the “c” lattice constant, 21.182 Å. While this product phase is not a perovskite, it does possess bismuth atoms coordinated to six anions in an octahedral geometry. This product phase will be discussed in greater detail in Chapter 6, “Discussion.”

Given that these three reactions gave rise to no unidentified peaks, it can be concluded that none of the hypothetical perovskites discussed in this paper were synthesized.

EXPERIMENTS 6, 8a, & 8b

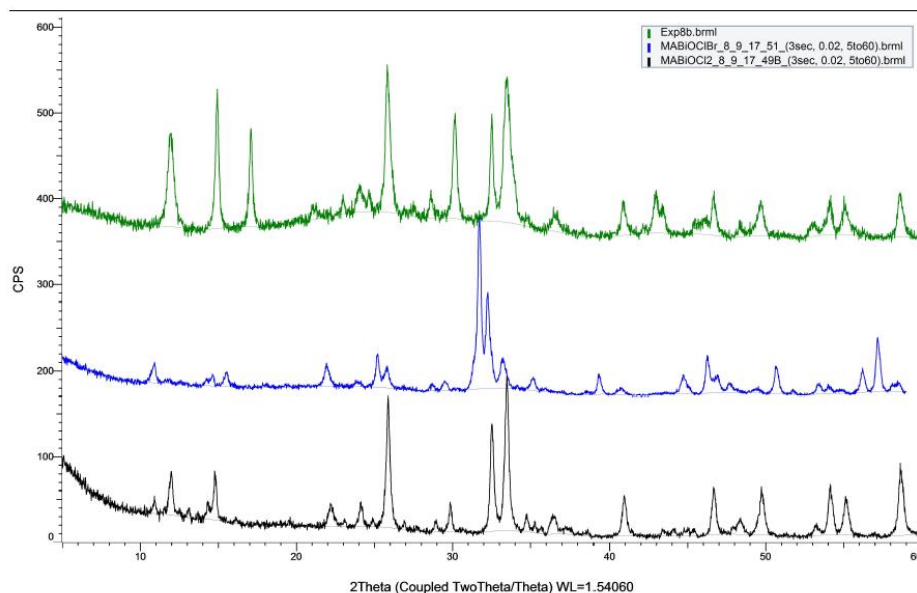


Figure 18 Comparison of XRD spectra demonstrating the effects of halide substitution:
(**BLACK**) Exp. 6: BiOCl & MACl (1 MA:1 Bi), 150°C, 3hrs.
(**BLUE**) Exp. 8a: BiOBr & MACl (1 MA:1 Bi) 150°C, 3 hrs.
(**GREEN**) Exp. 8b: BiOI & MACl (1 MA:1 Bi), 150°C, 3 hrs.

To compliment the previous BiOX & CsCl reactions, experiments 6, 8a, and 8b elucidated the reaction of bismuth oxyhalide compounds with the organic salt, methylammonium chloride, (CH₃NH₃)Cl (abbreviated to MACl). Analysis of the heated BiOCl and MACl sample (Experiment 6) resulted in an 87% match for unreacted BiOCl, the disappearance of the MACl salt, and the appearance of new unidentified peaks. Excel calculations designed to determine the number of new phases and label the peaks with corresponding hkl values was conducted (Appendix A). The new peaks corresponded to an orthorhombic unit cell with lattice constants a

(13.834 Å), b (8.108 Å), and c (6.756 Å). Careful scrutiny of the peak angles of the unidentified peaks failed to match the peak angles of the hypothetical bismuth oxyhalide perovskites tabulated in Table 4 to any significant degree.

The reaction of BiOBr and MAcl (Experiment 8a) resulted in a significant amount of unreacted BiOBr, as well as several unidentified peaks. Lattice parameter fitting was done in Excel (Appendix A) and showed two new phases unrelated to the one identified in Experiment 6. The first of these two new phases was found to have lattice parameters: a (6.198 Å), b (6.055 Å), and c (5.706 Å), the second: a (3.724 Å), b (3.697 Å), and c (3.450 Å), respectively. Once again, an analysis of the peak angles of the unidentified peaks failed to match the peak angles of the hypothetical bismuth oxyhalide perovskites tabulated in Table 4 to any significant degree.

The sample of heated BiOI and MAcl was analyzed, matching the peaks for unreacted MAcl, but it did not reveal traces of unreacted BiOI. Instead, a 91% match for BiOCl was observed, possibly indicating a halide-swap reaction between the methylammonium salt and the bismuth oxyhalide. As was the case with the cesium chloride reactions, the bismuth oxyiodide compound reacts much more readily at these experimental conditions, possibly indicating an enhanced likelihood of perovskite formation as well. As is shown in the Excel table in Appendix A, the unidentified peaks of this spectrum do not correspond to a significantly sufficient degree to conclude the formation of any of the hypothetical bismuth oxyhalide compounds discussed previously.

EXPERIMENTS 12, 17, 18, & 19

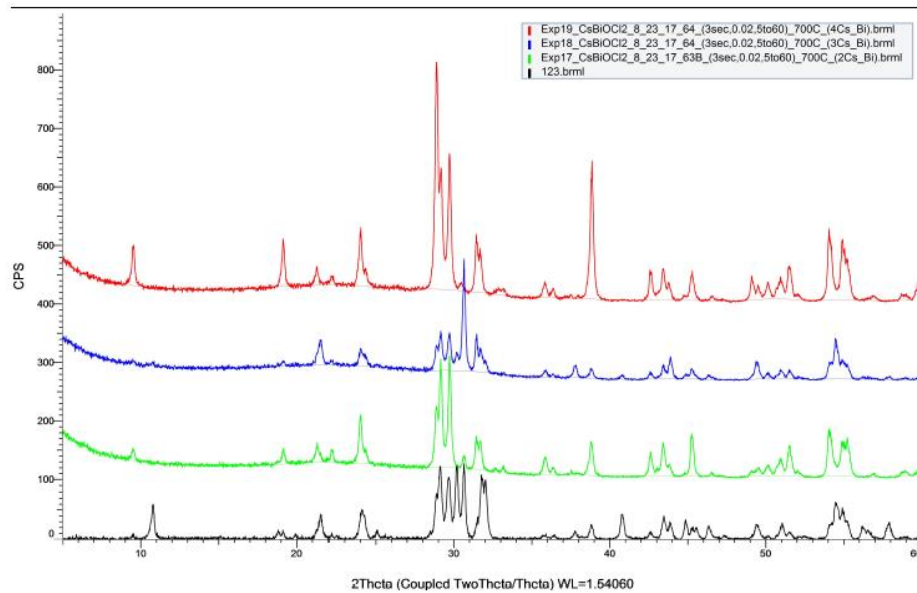


Figure 19 Comparison of XRD spectra demonstrating the effect of variable cation ratio at high temperatures:
(**BLACK**) Exp. 12: BiOCl & CsCl, (1 Cs:1 Bi), 700°C, 22 hrs.
(**GREEN**) Exp. 17: BiOCl & CsCl, (2 Cs:1 Bi), 700°C, 21.5 hrs.
(**BLUE**) Exp. 18: BiOCl & CsCl, (3 Cs:1 Bi), 700°C, 21.5 hrs.
(**RED**) Exp. 19: BiOCl & CsCl, (4 Cs:1 Bi), 700°C, 21.5 hrs.

Once reactions of each bismuth oxyhalide compound (BiOX) with cesium chloride and methylammonium chloride were conducted, it was time to vary experimental parameters and gauge their effect on the resulting samples. The first factor to be varied was the cation ratio of cesium to bismuth, in other words, the ratio of the initial reactants. Additionally, the temperature was increased to 700°C in an attempt to enhance the reactivity of cesium ions and increase their mobility, considering it has a melting point of 645°C, and would therefore be a liquid while

heated. The methylammonium analogs of these compounds were not attempted because the organic methylammonium atom is known to break down at temperatures above 231 °C.

The reaction of equal molar cesium chloride and bismuth oxychloride at the above-specified conditions resulted in a reaction between BiOCl molecules only. These reactions led to the production of such phases as $B_{24}O_{31}Cl_{10}$ (87% match) and B_3O_4Cl (72% match). There was no discernable evidence of unreacted cesium chloride or cesium-containing species left in the product.

Using twice as many moles of cesium chloride as bismuth oxychloride resulted in the complete conversion of all BiOCl to Bi_3O_4Cl (89% match). This time, cesium chloride was observed, evidenced most notably by the small peak at $\sim 30.653^\circ$ (2θ).

A 3:1 ratio of cesium chloride to bismuth oxychloride resulted in Bi_3O_4Cl and a significant amount of unreacted cesium chloride, so much so that its [110] reflection peak has the highest intensity of the spectrum.

Four times as much cesium chloride as bismuth oxychloride resulted in mostly Bi_3O_4Cl with a trace amount of unreacted cesium chloride.

These experiments show that increasing the amount of cesium chloride present generally results in a greater amount of unreacted cesium chloride, not an increased degree of reaction. It is also evident that high temperatures lead to the reaction of BiOCl with itself, causing the formation of phases like Bi_3O_4Cl and $B_{24}O_{31}Cl_{10}$. Moving forward, such high temperatures will be avoided, as they evidently do not promote favorable reactions of the reactants.

Seeing as all peaks had been accounted for, there was no reason to believe that the hypothetical perovskites of interest had been synthesized.

EXPERIMENTS 24, 25a, 25b, & 25c

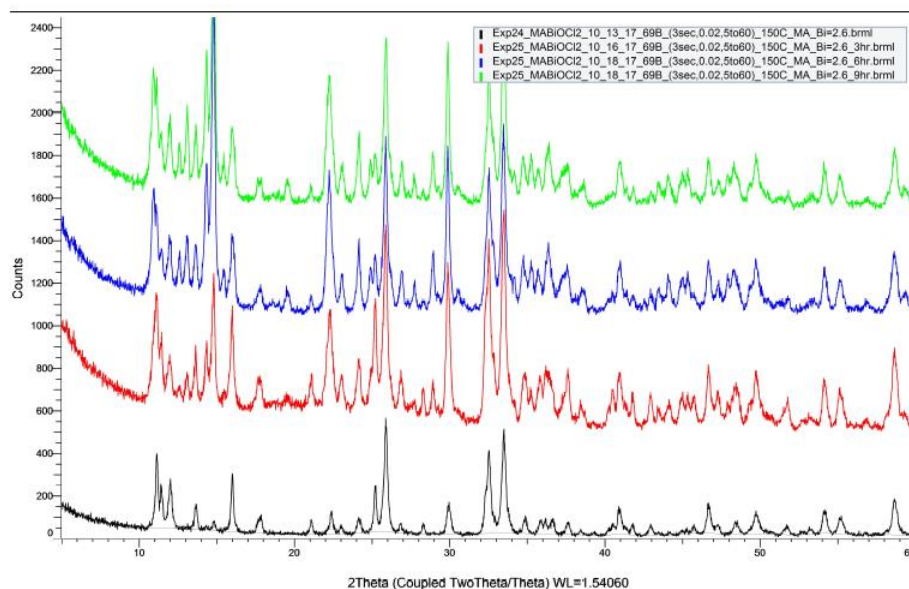


Figure 20 Comparison of XRD spectra demonstrating the effect of heating duration:
(**BLACK**) Exp 24: BiOCl & MACl (2.6 MA:1 Bi), 150°C, 1hrs.
(**RED**) Exp 25a: BiOCl & MACl (2.6 MA:1 Bi) 150°C, 3 hrs.
(**BLUE**) Exp 25b: BiOCl & MACl (2.6 MA:1 Bi), 150°C, 6 hrs.
(**GREEN**) Exp 25c: BiOCl & MACl (2.6 MA:1 Bi), 150°C, 9 hrs.

Having studied the effect of cation molar ratio on the reactions of interest, it was also desired to understand how the duration of heating influenced the products observed. In the reaction of BiOCl and MACl heated for one, three, six, and nine hours, a significant number of unidentified peaks were observed, along with peaks corresponding to unreacted BiOCl. One reason that the multitude of new peaks could be observed would be due to the cation ratio of 2.6. Making the methylammonium concentration so much greater than the bismuth concentration was done purposefully

in an effort to promote the reaction of BiOCl, which was still found in its unreacted form.

Though peaks corresponding to MACl might have been concealed by the large number of other peaks in this spectrum, there was little evidence to suggest that unreacted MACl was present in the sample. The cesium analogs of these compounds were not attempted due to the fact that the temperature of heating for these experiments was so far below the melting points of the two reactants that reaction was not likely, as evidenced by experiments 5, 7a, and 7b.

Excel calculations (Appendices A) confirmed the presence of one phase present in each of the samples analyzed. The lattice constants fit to the XRD peaks provided are shown below in Table 6 below. Note the minor variability between these values.

Experiments	“a” (Å)	“b” (Å)	“c” (Å)
Exp 24: 1-hour	7.936	7.744	6.478
Exp 25a: 3-hour	7.969	7.769	6.495
Exp 25b: 6-hour	7.985	7.753	6.488
Exp 25c: 9-hour	7.976	7.767	6.485

Table 6 Summary of the lattice constants derived for one phase found in four samples heated at the same temperature and composition for varying amounts of time.

Carefully comparison between the peak angle values summarized in Table 4 and the spectra of the products for these four experiments did not provide compelling evidence to believe that the hypothetical bismuth oxyhalide proposed in this work had been synthesized.

EXPERIMENTS 26a & 26b

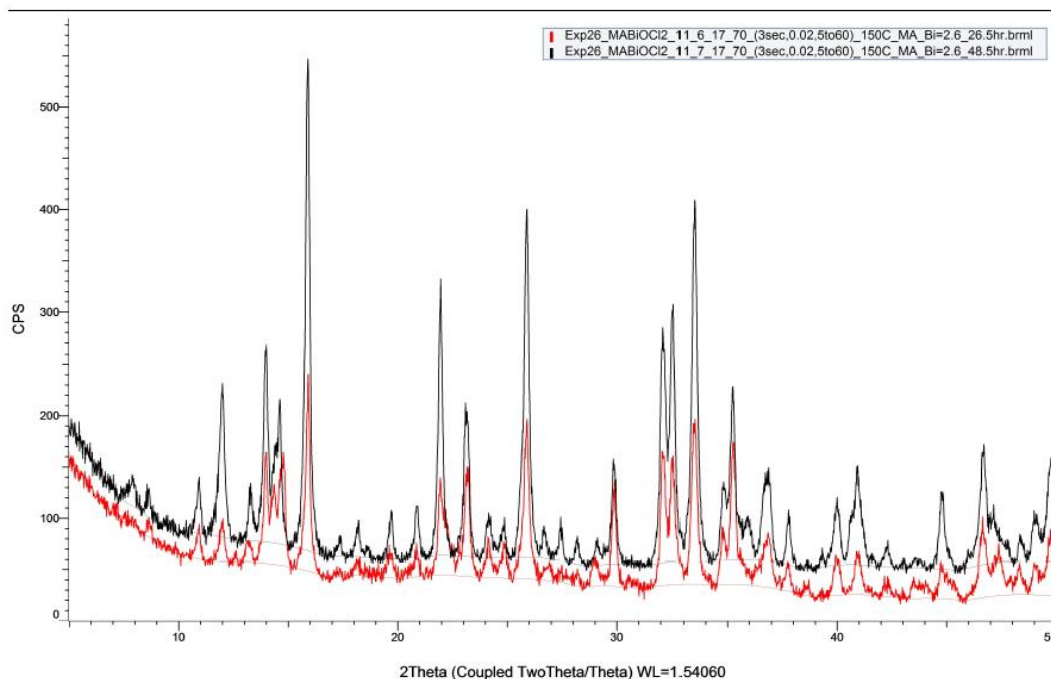


Figure 21 Comparison of XRD spectra demonstrating the effects of heating duration:
(**RED**) Exp 26a: BiOCl & MACl (2.6 MA:1 Bi) 150°C, 26.5 hrs.
(**BLACK**) Exp 26b: BiOCl & MACl (2.6 MA:1 Bi), 150°C, 48.5 hrs.

Having just analyzed the heating durations for BiOCl & MACl reactions between one to nine hours, longer-term heating times of 26.5 and 48.5 hours were also studied. The most striking feature of these spectra was the 90% match for a compound known as methylammonium nonachlorodibismuthate(III), or $\text{MA}_3\text{Bi}_2\text{Cl}_9$, which is structurally similar to the cesium nonaiododibismuthate(III) compound, $\text{Cs}_3\text{Bi}_2\text{I}_9$, observed in experiment 7b. $\text{MA}_3\text{Bi}_2\text{Cl}_9$ possesses in an orthorhombic crystal system with Pnma space group and lattice constants a (20.406 Å), b (7.7 Å), and c (13.246 Å).

The intensity of the new $\text{MA}_3\text{Bi}_2\text{Cl}_9$ phase is seen to be increase between the 26.5 and 48.6-hour patterns. Because increased intensity is correlated to an increased amount of a compound present, the increase in intensity is taken to mean that there was a greater amount of $\text{MA}_3\text{Bi}_2\text{Cl}_9$ present in the sample heated for 48.5 hours.

Despite the striking number of peaks in these spectra, all reflections were accounted for. As a result, no unidentified peaks were available to be compared to the tabulated values for peak angles in Table 4. It was therefore concluded that the hypothetical compounds of interest were not synthesized in experiments 26a or 26b.

EXPERIMENTS 27, 28, 29, & 30

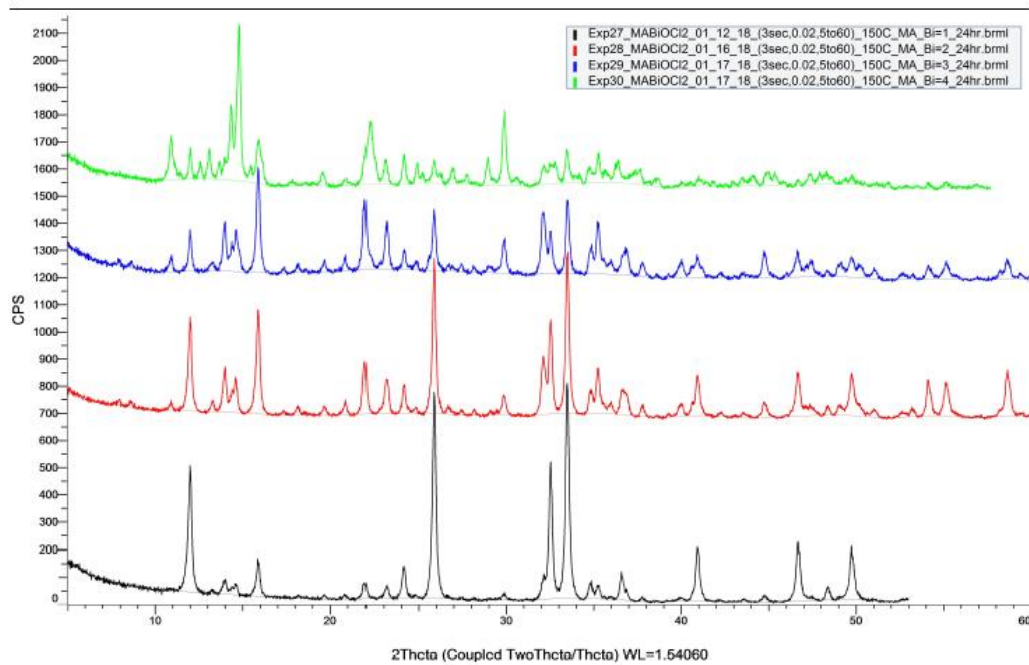


Figure 22 Comparison of XRD spectra demonstrating the effects of variable cation ratio:

(BLACK) BiOCl & MAcl (1 MA:1 Bi), 150°C, 24hrs.

(RED) BiOCl & MAcl (2 MA:1 Bi) 150°C, 24 hrs.

(BLUE) BiOCl & MAcl (3 MA:1 Bi), 150°C, 24 hrs.

(GREEN) BiOCl & MAcl (4 MA:1 Bi), 150°C, 24 hrs.

Experiments 27 through 30 were designed to gauge the effect of increasing cation ratio on the identity of the products formed. The XRD spectra for each of these samples contained unreacted BiOCl, while none provided evidence of unreacted MAcl—indicating that it must have reacted or volatilized away during heating. Also present in each of these samples was a significant amount of the $\text{MA}_3\text{Bi}_2\text{Cl}_9$ compound just discussed (see Appendix B).

For the molar reactant ratios 1:1 through 3:1, the intensity of peaks related to $\text{MA}_3\text{Bi}_2\text{Cl}_9$ continues grew steadily as a function of cation molar ratio. Every peak was accounted for in experiments 27, 28, and 29. Experiment 30 demonstrated signs of unreacted BiOCl and product $\text{MA}_3\text{Bi}_2\text{Cl}_9$, but this sample also contained new, unidentified peaks. Excel was used (Appendix A) to fit these peaks to a crystal with lattice constants a (7.775 Å), b (7.032 Å), and c (6.468 Å). Note that these values line up quite closely with the family of lattice constants identified in experiments 24 through 25c. Unfortunately, they do not match to any significant degree the values proposed for the hypothetical bismuth oxyhalide compounds proposed in this paper.

Chapter 6

DISCUSSION

While it was not possible to demonstrate the formation of three-dimensional perovskite compounds, a photoactive product was observed, as evidenced by experiments 5, 27, 28, 29, and 30. These products included $\text{Cs}_3\text{Bi}_2\text{I}_9$ ⁴⁴ and $(\text{CH}_3\text{NH}_3)_3\text{Bi}_2\text{Cl}_9$,⁴⁵ depicted schematically below in Figure 23.

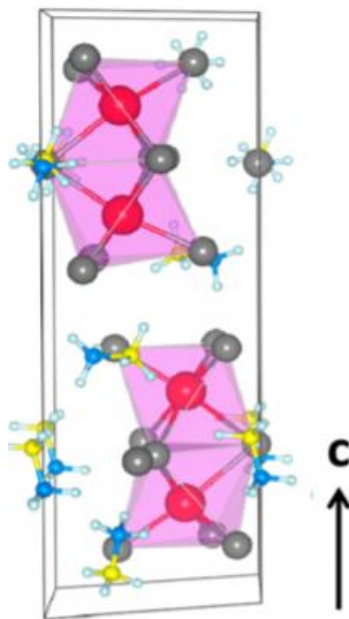


Figure 23 A visualization of the $\text{A}_3\text{B}_2\text{X}_9$ unit cell, wherein the red atoms represent Bismuth B-site, grey represent halide atoms, and the blue-yellow molecules represent methylammonium or cesium.⁴⁶

Research into the photovoltaic properties of these compounds has been carried out and power conversion efficiencies as high as 1% have been reported.⁴⁷ While this

efficiency is far lower than the most state-of-the-art compounds revolutionizing the field of PSCs, the ability to synthesize inexpensive, nontoxic, photoactive compounds is surely not without its merits.

Because the hypothetical bismuth oxyhalide compounds proposed in this research thesis were not observed, it was not possible to discern from experimental data whether those hypothetical compounds would be expected to hybridize. However, it is insightful to note that the presence of bismuth coordinated to the halide anions in an octahedral geometry of the $\text{Cs}_3\text{Bi}_2\text{I}_9$ and $(\text{CH}_3\text{NH}_3)_3\text{Bi}_2\text{Cl}_9$ compounds demonstrates that bismuth hybridization does not, in fact, occur! Had the $6s^2$ -lone pair of electrons hybridized, significant structural distortions and nonorthogonal angles of the bismuth coordination environments would have been observed. Absence of these distortions allows us to conclude that hybridization did not occur.

Chapter 7

CONCLUSIONS

The foregoing research discussed attempts to synthesize a new family of hypothetical photovoltaic bismuth compounds for applications in perovskite solar cells, namely $(\text{CH}_3\text{NH}_3)\text{BiOCl}_2$, $(\text{CH}_3\text{NH}_3)\text{BiOBr}_2$, $(\text{CH}_3\text{NH}_3)\text{BiOI}_2$, $(\text{CH}_3\text{NH}_3)\text{BiOClBr}$, $(\text{CH}_3\text{NH}_3)\text{BiOBrI}$, and $(\text{CH}_3\text{NH}_3)\text{BiOClI}$, and their cesium analogs CsBiOCl_2 , CsBiOBr_2 , CsBiOI_2 , CsBiOClBr , CsBiOBrI , and CsBiOClI . Fundamental geometry was employed to predict the feasibility of these hypothetical compounds by way of tolerance factor and lattice constant calculations. With these values in hand, it was possible to predict the hypothetical X-ray Powder Diffraction spectra that would be associated with these compounds, as well as the effect that octahedral tilting distortions would have on the hypothetical lattice constants of these compounds.

Experimental attempts to synthesize said compounds were attempted at a variety of conditions, varying temperature, heat duration, and the molar ratio of reactants, specifically. While it was not possible to produce three-dimensional bismuth oxyhalide perovskites, synthesis of the photoactive compounds $\text{Cs}_3\text{Bi}_2\text{I}_9$ and $(\text{CH}_3\text{NH}_3)_3\text{Bi}_2\text{Cl}_9$ were successful, if unintentional.

There are many reasons that could be to blame for why the compounds of interest could not be synthesized at the reaction conditions mentioned—such as the choice to use a dry-experimental synthesis procedure or the emphasis of bismuth oxychloride over other bismuth oxyhalides like bromide or iodide. Moving forward, it

would be advantageous to study the synthesis of the hypothetical bismuth oxyhalide compounds involving a greater focus on bismuth oxyiodide reactions with methylammonium chloride, considering several literature articles discussing their enhanced feasibility for perovskite formation,^{38,48,47} and evidence presented here in experiments 5 & 6 speaking to their enhanced reactivity. All reactions with cesium chloride should be discontinued, given that both hypothetical and experimental evidence indicates the unlikelihood of perovskite formation from cesium salts. A high cation molar ratio is recommended to promote reaction of the two reagents while temperatures in excess of 150°C but below 210°C are cautiously suggested. Heating durations in excess of three hours are also encouraged in order to facilitate reaction of the chemical species.

REFERENCES

1. Krebs FC, Spanggard H, Kjær T, Biancardo M, Alstrup J. Large area plastic solar cell modules. *Mater Sci Eng B Solid-State Mater Adv Technol.* 2007;138(2):106-111. doi:10.1016/j.mseb.2006.06.008
2. Yang WS, Park B-W, Jung EH, Jeon NJ. Iodide management in formamidinium-lead-halide – based perovskite layers for efficient solar cells. *Science (80-)*. 2017;356(6345):1376-1379. doi:10.1126/science.aan2301
3. Giustino F, Snaith HJ. Toward Lead-Free Perovskite Solar Cells. *ACS Energy Lett.* 2016;1(6):1233-1240. doi:10.1021/acsenergylett.6b00499
4. Ribeyron P-J. Crystalline silicon solar cells: Better than ever. *Nat Energy.* 2017;2(5):17067. doi:10.1038/nenergy.2017.67
5. Seo J, Park S, Chan Kim Y, et al. Benefits of very thin PCBM and LiF layers for solution-processed p–i–n perovskite solar cells. *Energy Environ Sci.* 2014;7(8):2642-2646. doi:10.1039/C4EE01216J
6. Kim HS, Park NG. Parameters affecting I-V hysteresis of CH₃NH₃PbI₃ perovskite solar cells: Effects of perovskite crystal size and mesoporous TiO₂ layer. *J Phys Chem Lett.* 2014. doi:10.1021/jz501392m
7. Hailegnaw B, Kirmayer S, Edri E, Hodes G, Cahen D. Rain on methylammonium lead iodide based perovskites: Possible environmental effects of perovskite solar cells. *J Phys Chem Lett.* 2015. doi:10.1021/acs.jpcclett.5b00504
8. Foyevtsova K, Khazraie A, Elfimov I, Sawatzky GA. Hybridization effects and bond disproportionation in the bismuth perovskites. *Phys Rev B - Condens Matter Mater Phys.* 2015;91(12):2-6. doi:10.1103/PhysRevB.91.121114
9. Mohn CE, Stølen S. Influence of the stereochemically active bismuth lone pair structure on ferroelectricity and photocatalytic activity of Aurivillius phase Bi₂WO₆. *Phys Rev B - Condens Matter Mater Phys.* 2011;83(1):1-7. doi:10.1103/PhysRevB.83.014103
10. Ghosh S, Dasgupta S, Sen A, Maiti HS. Low temperature synthesis of bismuth ferrite nanoparticles by a ferrioxalate precursor method. *Mater Res Bull.* 2005;40(12):2073-2079. doi:10.1016/j.materresbull.2005.07.017

11. Liu J, Xue Y, Wang Z, et al. Two-Dimensional CH₃NH₃PbI₃ Perovskite: Synthesis and Optoelectronic Application. *ACS Nano*. 2016. doi:10.1021/acsnano.5b07791
12. Klug MT, Osherov A, Haghighirad AA, et al. Tailoring metal halide perovskites through metal substitution: influence on photovoltaic and material properties. *Energy Environ Sci*. 2017;10(1):236-246. doi:10.1039/C6EE03201J
13. Noel NK, Stranks SD, Abate A, et al. Lead-free organic–inorganic tin halide perovskites for photovoltaic applications. *Energy Environ Sci*. 2014. doi:10.1039/C4EE01076K
14. Frolova LA, Anokhin D V., Gerasimov KL, Dremova NN, Troshin PA. Exploring the Effects of the Pb²⁺ Substitution in MAPbI₃ on the Photovoltaic Performance of the Hybrid Perovskite Solar Cells. *J Phys Chem Lett*. 2016;7(21):4353-4357. doi:10.1021/acs.jpcclett.6b02122
15. Volonakis G, Filip MR, Haghighirad AA, et al. Lead-Free Halide Double Perovskites via Heterovalent Substitution of Noble Metals. *J Phys Chem Lett*. 2016;7(7):1254-1259. doi:10.1021/acs.jpcclett.6b00376
16. Abdelhady AL, Saidaminov MI, Murali B, et al. Heterovalent Dopant Incorporation for Bandgap and Type Engineering of Perovskite Crystals. *J Phys Chem Lett*. 2016;7(2):295-301. doi:10.1021/acs.jpcclett.5b02681
17. Mosconi E, Merabet B, Meggiolaro D, Zaoui A, De Angelis F. First-Principles Modeling of Bismuth Doping in the MAPbI₃ Perovskite. *J Phys Chem C*. 2018:acs.jpcc.8b01307. doi:10.1021/acs.jpcc.8b01307
18. Akkerman QA, D’Innocenzo V, Accornero S, et al. Tuning the optical properties of cesium lead halide perovskite nanocrystals by anion exchange reactions. *J Am Chem Soc*. 2015;137(32):10276-10281. doi:10.1021/jacs.5b05602
19. Ganose AM, Cuff M, Butler KT, Walsh A, Scanlon DO. Interplay of Orbital and Relativistic Effects in Bismuth Oxyhalides: BiOF, BiOCl, BiOBr, and BiOI. *Chem Mater*. 2016. doi:10.1021/acs.chemmater.6b00349
20. Zhang KL, Liu CM, Huang FQ, Zheng C, Wang WD. Study of the electronic structure and photocatalytic activity of the BiOCl photocatalyst. *Appl Catal B Environ*. 2006. doi:10.1016/j.apcatb.2006.08.002

21. Ye P, Xie J, He Y, Zhang L, Wu T, Wu Y. Hydrolytic synthesis of flowerlike BiOCl and its photocatalytic performance under visible light. *Mater Lett*. 2013;108:168-171. doi:10.1016/j.matlet.2013.06.059
22. Gnayem H, Sasson Y. Hierarchical nanostructured 3D flowerlike BiOCl_xBr_{1-x} semiconductors with exceptional visible light photocatalytic activity. *ACS Catal*. 2013;3(2):186-191. doi:10.1021/cs3005133
23. Yin WJ, Shi T, Yan Y. Unique properties of halide perovskites as possible origins of the superior solar cell performance. *Adv Mater*. 2014. doi:10.1002/adma.201306281
24. Amat A, Mosconi E, Ronca E, et al. Cation-induced band-gap tuning in organohalide perovskites: Interplay of spin-orbit coupling and octahedra tilting. *Nano Lett*. 2014;14(6):3608-3616. doi:10.1021/nl5012992
25. Baikie T, Fang Y, Kadro JM, et al. Synthesis and crystal chemistry of the hybrid perovskite (CH₃NH₃)PbI₃ for solid-state sensitised solar cell applications. *J Mater Chem A*. 2013;1(18):5628. doi:10.1039/c3ta10518k
26. Travis W, Glover ENK, Bronstein H, Scanlon DO, Palgrave RG. On the application of the tolerance factor to inorganic and hybrid halide perovskites: a revised system. *Chem Sci*. 2016;7(7):4548-4556. doi:10.1039/C5SC04845A
27. Glazer AM. Simple ways of determining perovskite structures. *Acta Crystallogr Sect A*. 1975;31(6):756-762. doi:10.1107/S0567739475001635
28. Cheng L-Q, Wang K, Li J-F. Synthesis of highly piezoelectric lead-free (K, Na)NbO₃ one-dimensional perovskite nanostructures. *Chem Commun*. 2013;49(38):4003. doi:10.1039/c3cc41371c
29. Wei F, Deng Z, Sun S, et al. Synthesis and Properties of a Lead-Free Hybrid Double Perovskite: (CH₃NH₃)₂AgBiBr₆. *Chem Mater*. 2017;29(3):1089-1094. doi:10.1021/acs.chemmater.6b03944
30. Smith IC, Hoke ET, Solis-Ibarra D, McGehee MD, Karunadasa HI. A Layered Hybrid Perovskite Solar-Cell Absorber with Enhanced Moisture Stability. *Angew Chemie - Int Ed*. 2014. doi:10.1002/anie.201406466
31. Tsai H, Nie W, Blancon J-C, et al. High-efficiency two-dimensional Ruddlesden–Popper perovskite solar cells. *Nature*. 2016. doi:10.1038/nature18306

32. Frit B, Mercurio JP. The crystal chemistry and dielectric properties of the Aurivillius family of complex bismuth oxides with perovskite-like layered structures. *J Alloys Compd.* 1992;188(C):27-35. doi:10.1016/0925-8388(92)90639-Q
33. Maeda K, Mallouk TE. Comparison of two- and three-layer restacked Dion–Jacobson phase niobate nanosheets as catalysts for photochemical hydrogen evolution. *J Mater Chem.* 2009;19(27):4813. doi:10.1039/b903692j
34. Kieslich G, Sun S, Cheetham AK. An extended Tolerance Factor approach for organic–inorganic perovskites. *Chem Sci.* 2015;6(6):3430-3433. doi:10.1039/C5SC00961H
35. Li Z, Yang M, Park JS, Wei SH, Berry JJ, Zhu K. Stabilizing Perovskite Structures by Tuning Tolerance Factor: Formation of Formamidinium and Cesium Lead Iodide Solid-State Alloys. *Chem Mater.* 2016;28(1):284-292. doi:10.1021/acs.chemmater.5b04107
36. Chen Q, Zhou H, Fang Y, et al. The optoelectronic role of chlorine in CH₃NH₃PbI₃(Cl)-based perovskite solar cells. *Nat Commun.* 2015. doi:10.1038/ncomms8269
37. Woodward PM. Octahedral Tilting in Perovskites. II. Structure Stabilizing Forces. *Acta Crystallogr Sect B Struct Sci.* 1997;53(1):44-66. doi:10.1107/S0108768196012050
38. Wheeler RA, Kumar PNVP. Stereochemically Active or Inactive Lone Pair Electrons in Some Six-Coordinate, Group 15 Halides. *J Am Chem Soc.* 1992;114(12):4776-4784. doi:10.1021/ja00038a049
39. Stoltzfus MW, Woodward PM, Seshadri R, Klepeis J, Bursten B. Inert Pairs. 2007;46(10):3839-3850. doi:10.1021/ic061157g
40. Morin E, Wallez G, Jaulmes S, Couturier JC, Querton M. Structure of PbII₂SnIV(PO₄)₂: Stereochemical Activity of the Lead II Lone Pair. *J Solid State Chem.* 1998;137(2):283-288. doi:10.1006/jssc.1997.7735
41. Seshadri R, Hill NA. Visualizing the role of Bi 6s “lone pairs” in the off-center distortion in ferromagnetic BiMnO₃. *Chem Mater.* 2001;13(9):2892-2899. doi:10.1021/cm010090m

42. Bi W, Leblanc N, Mercier N, Auban-Senzier P, Pasquier C. Thermally induced Bi(III) lone pair stereoactivity: Ferroelectric phase transition and semiconducting properties of (MV)BiBr₅ (MV = methylviologen). *Chem Mater*. 2009;21(18):4099-4101. doi:10.1021/cm9016003
43. Blackman M, Khan IH. The polymorphism of thallium and other halides at low temperatures. *Proc Phys Soc*. 1961;77(2):471-475. doi:10.1088/0370-1328/77/2/331
44. Park BW, Philippe B, Zhang X, Rensmo H, Boschloo G, Johansson EMJ. Bismuth Based Hybrid Perovskites A₃Bi₂I₉ (A: Methylammonium or Cesium) for Solar Cell Application. *Adv Mater*. 2015;27(43):6806-6813. doi:10.1002/adma.201501978
45. Diffraction X, Scattering R. *zl*. 1. 1993;45:45-56.
46. Timmermans CWM, Blasse G. On the Luminescence of Cs₃Bi₂Br₉ Single Crystals. *Phys Status Solidi*. 1981;106(2):647-655. doi:10.1002/pssb.2221060230
47. Pazoki M, Johansson MB, Zhu H, et al. Bismuth Iodide Perovskite Materials for Solar Cell Applications: Electronic Structure, Optical Transitions, and Directional Charge Transport. *J Phys Chem C*. 2016;120(51):29039-29046. doi:10.1021/acs.jpcc.6b11745
48. Sun S, Tominaka S, Lee JH, Xie F, Bristowe PD, Cheetham AK. Synthesis, crystal structure, and properties of a perovskite-related bismuth phase, (NH₄)₃Bi₂I₉. *APL Mater*. 2016;4(3). doi:10.1063/1.4943680

APPENDIX A: EXCEL LATTICE CONSTANT FITTING

EXPERIMENT 6

2θ	d	h	k	l	d	2θ	Δ2θ		
6.384	13.834	1	0	0	13.834	6.389	-0.005	a	13.834
10.903	8.108	0	1	0	8.108	10.912	-0.009	b	8.108
13.093	6.756	0	0	1	6.756	13.103	-0.010	c	6.756
14.369	6.159	-	-	-	-	-	-		
14.796	5.982	1	0	1	6.071	14.590	0.206		
16.121	5.494	2	1	0	5.262	16.848	-0.727		
22.227	3.996	3	1	0	4.008	22.177	0.050		
23.091	3.849	3	0	1	3.809	23.355	-0.264		
24.894	3.574	-	-	-	-	-	-		
26.906	3.311	1	2	1	3.371	26.436	0.470		
28.940	3.083	4	0	1	3.079	29.003	-0.063		
29.868	2.989	2	0	2	3.036	29.424	0.444		
35.272	2.543	1	2	2	2.551	35.182	0.090		
35.688	2.514	2	3	0	2.517	35.665	0.023		
36.501	2.460	1	3	1	2.469	36.387	0.114		
36.500	2.460	4	2	1	2.452	36.652	-0.152		
37.513	2.396	4	0	2	2.417	37.204	0.309		
38.625	2.329	3	3	0	2.332	38.612	0.013		
44.092	2.052	2	1	3	2.070	43.718	0.374		
44.990	2.013	2	3	2	2.019	44.904	0.086		
45.388	1.997	1	4	0	2.006	45.210	0.178		
47.973	1.895	4	0	3	1.887	48.218	-0.245		
48.064	1.892	2	2	3	1.894	48.048	0.016		

EXPERIMENT 7b

2θ	d	h	k	l	d	2θ	$\Delta(2\theta)$		
12.824	6.898	1	0	0	6.898	12.834	-0.010	a	6.898
27.000	3.300	0	2	0	3.300	27.021	-0.021	b	6.599
27.527	3.238	0	0	2	3.238	27.549	-0.022	c	6.475
28.376	3.143	1	0	0	6.898	12.834	15.542		
28.381	3.142	0	1	0	6.599	13.416	14.965	a'	3.143
29.729	3.003	1	2	0	2.977	30.019	-0.290	b'	3.142
31.767	2.815	0	0	1	6.475	13.675	18.092	c'	2.815
42.998	2.102	1	3	0	2.096	43.164	-0.166		
45.598	1.988	1	3	1	1.994	45.488	0.110		
49.643	1.835	2	0	3	1.830	49.837	-0.194		

EXPERIMENT 8a

2θ	d	h	k	l	d	2θ	$\Delta 2\theta$		
14.279	6.198	1	0	0	6.198	14.290	-0.011	a	6.198
14.618	6.055	0	1	0	6.055	14.630	-0.012	b	6.055
15.518	5.706	0	0	1	5.706	15.530	-0.012	c	5.706
23.877	3.724	1	0	0	3.724	23.896	-0.019		
24.054	3.697	0	1	0	3.697	24.073	-0.019	a'	3.724
25.803	3.450	0	0	1	3.450	25.824	-0.021	b'	3.697
28.726	3.105	2	0	0	3.099	28.808	-0.082	c'	3.450
29.529	3.023	0	2	0	3.027	29.505	0.024		
33.223	2.695	0	2	1	2.674	33.509	-0.286		
34.12	2.626	1	0	2	2.591	34.612	-0.492		
35.156	2.551	0	1	2	2.581	34.762	0.394		
38.607	2.330	1	2	1	2.455	36.596	2.011		
40.746	2.213	-	-	-	-	-	-		
44.742	2.024	2	2	1	2.025	44.762	-0.020		
44.98	2.014	0	3	0	2.018	44.911	0.069		
49.478	1.841	3	1	1	1.850	49.262	0.216		
54.067	1.695	2	3	0	1.691	54.237	-0.170		
58.176	1.584	1	3	2	1.592	57.913	0.263		
58.501	1.576	2	1	3	1.566	58.988	-0.487		

EXPERIMENT 8b

2θ	d	h	k	l	d	2θ	$\Delta 2\theta$		
14.923	5.93162	1	0	0	5.932	14.935	-0.012	a	5.932
17.086	5.18555	0	1	0	5.186	17.099	-0.013	b	5.186
21.067	4.21369	0	0	1	4.214	21.083	-0.016	c	4.214
23.001	3.86362	1	1	0	3.904	22.777	0.224		
24.657	3.60767	1	0	1	3.435	25.937	-1.280		
27.538	3.23643	0	1	1	3.270	27.270	0.268		
28.634	3.11499	1	1	1	2.864	31.232	-2.598		
30.156	2.9612	2	0	0	2.966	30.132	0.024		
42.972	2.10305	0	0	2	2.107	42.926	0.046		
43.382	2.08413	0	1	2	1.952	46.526	-3.144		
46.106	1.96713	2	2	0	1.952	46.523	-0.417		
55.09	1.6657	3	1	1	1.692	54.210	0.880		

EXPERIMENT 24

2θ	d	h	k	l	d	2θ	Δ2θ		
11.140	7.936	1	0	0	7.936	11.149	-0.009	a	7.936
11.417	7.744	0	1	0	7.744	11.426	-0.009	b	7.744
13.658	6.478	0	0	1	6.478	13.669	-0.011	c	6.478
14.816	5.974	-	-	-	-	-	-		
16.000	5.535	1	1	0	5.542	15.990	0.010		
17.786	4.983	0	1	1	4.969	17.851	-0.065		
21.095	4.208	1	1	1	4.211	21.095	0.000		
22.382	3.969	-	-	-	-	-	-		
23.015	3.861	0	2	0	3.872	22.968	0.047		
25.207	3.530	2	1	0	3.531	25.218	-0.011		
26.841	3.319	0	2	1	3.324	26.824	0.017		
28.308	3.150	-	-	-	-	-	-		
29.947	2.981	0	1	2	2.988	29.901	0.046		
35.872	2.501	3	1	0	2.503	35.872	0.000		
36.163	2.482	0	2	2	2.484	36.155	0.008		
37.618	2.389	2	1	2	2.387	37.684	-0.066		
38.441	2.340	3	1	1	2.335	38.555	-0.114		
39.309	2.290	1	3	1	2.295	39.247	0.062		
40.284	2.237	-	-	-	-	-	-		
40.537	2.224	-	-	-	-	-	-		
41.777	2.160	2	3	0	2.164	41.743	0.034		
42.957	2.104	2	2	2	2.106	42.951	0.006		
44.986	2.014	0	3	2	2.019	44.901	0.085		
45.265	2.002	1	1	3	2.012	45.057	0.208		
45.720	1.983	4	0	0	1.984	45.730	-0.010		
47.247	1.922	4	1	0	1.922	47.295	-0.048		
48.448	1.877	1	4	0	1.881	48.393	0.055		
51.733	1.766	4	2	0	1.766	51.774	-0.041		
58.182	1.584	0	1	4	1.585	58.197	-0.015		

EXPERIMENT 25a

2θ	d	h	k	l	d	2θ	$\Delta 2\theta$		
11.094	7.969	1	0	0	7.969	11.103	-0.009	a	7.969
11.380	7.769	0	1	0	7.769	11.389	-0.009	b	7.769
12.582	7.030	-	-	-	-	-	-	c	6.495
13.072	6.767	-	-	-	-	-	-		
13.623	6.495	0	0	1	6.495	13.633	-0.010		
14.339	6.172	-	-	-	-	-	-		
14.782	5.988	-	-	-	-	-	-		
15.503	5.711	-	-	-	-	-	-		
15.984	5.540	1	1	0	5.563	15.931	0.053		
17.745	4.994	0	1	1	4.983	17.799	-0.054		
21.083	4.211	1	1	1	4.225	21.026	0.057		
22.287	3.986	2	0	0	3.984	22.312	-0.025		
23.032	3.858	0	2	0	3.885	22.892	0.140		
24.997	3.559	0	0	2	3.247	27.465	-2.468		
25.197	3.532	2	1	0	3.545	25.117	0.080		
26.872	3.315	0	2	1	3.334	26.740	0.132		
27.706	3.217	0	0	2	3.247	27.465	0.241		
28.300	3.151	-	-	-	-	-	-		
28.936	3.083	1	2	1	3.076	29.033	-0.097		
29.899	2.986	0	1	2	2.996	29.819	0.080		
32.507	2.752	2	2	0	2.781	32.181	0.326		
34.124	2.625	3	0	0	2.656	33.742	0.382		
35.227	2.546	2	2	1	2.557	35.096	0.131		
35.839	2.504	3	1	0	2.513	35.722	0.117		
36.258	2.476	0	2	2	2.492	36.047	0.211		
37.613	2.389	2	1	2	2.395	37.558	0.055		
38.465	2.338	3	1	1	2.344	38.401	0.064		
40.264	2.238	-	-	-	-	-	-		
40.501	2.226	-	-	-	-	-	-		
41.794	2.160	0	0	3	2.165	41.719	0.075		
42.946	2.104	2	2	2	2.113	42.806	0.140		
43.468	2.080	0	1	3	2.085	43.388	0.080		
44.125	2.051	3	0	2	2.056	44.041	0.084		
44.963	2.014	1	1	3	2.018	44.927	0.036		
45.340	1.999	4	0	0	1.992	45.530	-0.190		
45.716	1.983	3	1	2	1.988	45.641	0.075		
47.277	1.921	4	1	0	1.930	47.091	0.186		

47.948	1.896	2	0	3	1.902	47.814	0.134
48.472	1.877	1	4	0	1.887	48.223	0.249
49.351	1.845	2	1	3	1.848	49.318	0.033
51.756	1.765	4	2	0	1.773	51.555	0.201
54.146	1.693	4	0	2	1.698	53.997	0.149
55.155	1.664	0	4	2	1.667	55.093	0.062
56.834	1.619	0	0	4	1.624	56.689	0.145
58.255	1.583	4	3	0	1.579	58.445	-0.190
58.662	1.573	4	3	0	1.579	58.445	0.217
59.302	1.557	1	1	4	1.559	59.285	0.017

EXPERIMENT 25b

2θ	d	h	k	l	d	2θ	$\Delta 2\theta$		
10.944	8.078	-	-	-	-	-	-	a	7.985
11.072	7.985	1	0	0	7.985	11.081	-0.009	b	7.753
11.403	7.753	0	1	0	7.753	11.412	-0.009	c	6.488
12.584	7.028	-	-	-	-	-	-		
13.081	6.763	-	-	-	-	-	-		
13.636	6.488	0	0	1	6.488	13.647	-0.011		
14.339	6.172	-	-	-	-	-	-		
14.782	5.988	-	-	-	-	-	-		
15.428	5.739	-	-	-	-	-	-		
16.024	5.526	1	1	0	5.562	15.933	0.091		
17.786	4.983	0	1	1	4.976	17.825	-0.039		
19.559	4.535	-	-	-	-	-	-		
21.094	4.208	1	1	1	4.223	21.036	0.058		
22.241	3.994	2	0	0	3.992	22.267	-0.026		
23.058	3.854	0	2	0	3.877	22.940	0.118		
24.921	3.570	-	-	-	-	-	-		
25.200	3.531	2	1	0	3.549	25.088	0.112		
26.915	3.310	0	2	1	3.328	26.788	0.127		
27.736	3.214	0	0	2	3.244	27.492	0.244		
28.312	3.150	-	-	-	-	-	-		
28.925	3.084	1	2	1	3.072	29.069	-0.144		
29.879	2.988	0	1	2	2.993	29.854	0.025		
30.540	2.925	-	-	-	-	-	-		
32.538	2.750	2	2	0	2.781	32.184	0.354		
34.126	2.625	-	-	-	-	-	-		
35.257	2.544	2	2	1	2.556	35.104	0.153		
35.702	2.513	3	1	0	2.517	35.665	0.037		
36.361	2.469	3	0	1	2.462	36.489	-0.128		
37.345	2.406	0	3	1	2.401	37.456	-0.111		
37.567	2.392	2	1	2	2.395	37.559	0.008		
38.554	2.333	3	1	1	2.347	38.353	0.201		
40.231	2.240	-	-	-	-	-	-		
40.958	2.202	3	2	0	2.194	41.138	-0.180		
41.364	2.181	-	-	-	-	-	-		
41.808	2.159	0	0	3	2.163	41.763	0.045		
42.565	2.122	-	-	-	-	-	-		
42.961	2.104	2	2	2	2.112	42.827	0.134		

43.466	2.080	0	1	3	2.083	43.436	0.030
44.115	2.051	3	0	2	2.058	44.005	0.110
44.981	2.014	1	1	3	2.016	44.968	0.013
45.339	1.999	4	0	0	1.996	45.436	-0.097
45.725	1.983	3	1	2	1.989	45.613	0.112
47.301	1.920	4	1	0	1.933	47.005	0.296
47.940	1.896	2	0	3	1.902	47.830	0.110
48.466	1.877	1	4	0	1.884	48.317	0.149
49.407	1.843	2	1	3	1.847	49.340	0.067
50.509	1.806	1	4	1	1.809	50.448	0.061
51.801	1.763	4	2	0	1.775	51.493	0.308
56.873	1.618	0	0	4	1.622	56.751	0.122
59.343	1.556	4	2	2	1.557	59.357	-0.014

EXPERIMENT 25c

2θ	d	h	k	l	d	2θ	$\Delta 2\theta$		
10.956	8.069	-	-	-	-	-	-	a	7.976
11.085	7.976	1	0	0	7.976	11.093	-0.008	b	7.767
11.384	7.767	0	1	0	7.767	11.393	-0.009	c	6.485
12.595	7.022	-	-	-	-	-	-		
13.086	6.760	-	-	-	-	-	-		
13.644	6.485	0	0	1	6.485	13.654	-0.010		
14.337	6.173	-	-	-	-	-	-		
14.783	5.988	-	-	-	-	-	-		
15.436	5.736	-	-	-	-	-	-		
16.003	5.534	-	-	-	-	-	-		
17.697	5.008	1	0	1	5.032	17.626	0.071		
17.790	4.982	0	1	1	4.978	17.818	-0.028		
19.552	4.537	-	-	-	-	-	-		
21.075	4.212	1	1	1	4.223	21.037	0.038		
22.242	3.994	2	0	0	3.988	22.293	-0.051		
23.061	3.854	0	2	0	3.883	22.900	0.161		
24.927	3.569	-	-	-	-	-	-		
25.202	3.531	2	1	0	3.548	25.102	0.100		
26.917	3.310	0	2	1	3.332	26.757	0.160		
27.735	3.214	0	0	2	3.242	27.508	0.227		
28.283	3.153	-	-	-	-	-	-		
28.927	3.084	2	1	1	3.112	28.683	0.244		
29.250	3.051	1	2	1	3.074	29.045	0.205		
29.883	2.988	0	1	2	2.992	29.860	0.023		
30.538	2.925	-	-	-	-	-	-		
32.699	2.736	-	-	-	-	-	-		
34.151	2.623	-	-	-	-	-	-		
35.251	2.544	-	-	-	-	-	-		
35.714	2.512	2	0	2	2.516	35.688	0.026		
36.348	2.470	1	3	0	2.462	36.488	-0.140		
37.304	2.409	0	3	1	2.404	37.401	-0.097		
37.558	2.393	2	1	2	2.393	37.580	-0.022		
38.610	2.330	-	-	-	-	-	-		
41.363	2.181	2	3	0	2.171	41.589	-0.226		
41.823	2.158	0	0	3	2.162	41.786	0.037		
42.995	2.102	2	2	2	2.111	42.828	0.167		
43.473	2.080	0	1	3	2.082	43.454	0.019		

44.098	2.052	3	0	2	2.056	44.046	0.052
44.897	2.017	0	3	2	2.023	44.796	0.101
45.017	2.012	1	1	3	2.015	44.989	0.028
45.343	1.998	4	0	0	1.994	45.490	-0.147
45.781	1.980	3	1	2	1.987	45.647	0.134
47.324	1.919	4	1	0	1.931	47.052	0.272
47.936	1.896	2	0	3	1.900	47.864	0.072
49.412	1.843	2	1	3	1.846	49.369	0.043
51.799	1.764	4	2	0	1.774	51.522	0.277
56.897	1.617	0	0	4	1.621	56.784	0.113
58.323	1.581	4	3	0	1.580	58.419	-0.096
59.328	1.556	1	1	4	1.557	59.376	-0.048

EXPERIMENT 30

2θ	d	h	k	l	d	2θ	$\Delta 2\theta$		
11.372	7.775	1	0	0	7.775	11.381	-0.009	a	7.775
12.578	7.032	0	1	0	7.032	12.588	-0.010	b	7.032
13.095	6.755	-	-	-	-	-	-	c	6.468
13.680	6.468	0	0	1	6.468	13.690	-0.010		
14.019	6.312	-	-	-	-	-	-		
14.346	6.169	-	-	-	-	-	-		
14.785	5.987	-	-	-	-	-	-		
15.463	5.726	-	-	-	-	-	-		
17.822	4.973	1	0	1	4.972	17.838	-0.016		
18.603	4.766	0	1	1	4.760	18.639	-0.036		
19.018	4.663	-	-	-	-	-	-		
22.235	3.995	-	-	-	-	-	-		
22.260	3.990	-	-	-	-	-	-		
22.526	3.944	2	0	0	3.887	22.876	-0.350		
24.157	3.681	-	-	-	-	-	-		
24.901	3.573	-	-	-	-	-	-		
25.200	3.531	0	2	0	3.516	25.332	-0.132		
26.208	3.398	2	1	0	3.402	26.193	0.015		
26.925	3.309	2	0	1	3.332	26.755	0.170		
27.734	3.214	1	2	0	3.204	27.849	-0.115		
28.943	3.082	0	2	1	3.089	28.903	0.040		
30.560	2.923	0	1	2	2.938	30.422	0.138		
30.892	2.892	1	2	1	2.871	31.155	-0.263		
32.756	2.732	1	1	2	2.748	32.578	0.178		
34.158	2.623	2	2	0	2.608	34.392	-0.234		
34.746	2.580	3	0	0	2.592	34.610	0.136		
35.650	2.516	-	-	-	-	-	-		
36.362	2.469	2	0	2	2.486	36.128	0.234		
37.612	2.390	0	2	2	2.380	37.795	-0.183		
38.630	2.329	0	3	0	2.344	38.403	0.227		
40.048	2.250	1	3	0	2.244	40.183	-0.135		
41.830	2.158	0	0	3	2.156	41.901	-0.071		
42.528	2.124	1	3	1	2.120	42.644	-0.116		
42.990	2.102	-	-	-	-	-	-		
43.498	2.079	1	0	3	2.078	43.561	-0.063		
44.116	2.051	-	-	-	-	-	-		
44.926	2.016	3	0	2	2.022	44.814	0.112		

45.357	1.998	1	1	3	1.992	45.525	-0.168
45.867	1.977	3	2	1	1.985	45.695	0.172
47.935	1.896	0	3	2	1.898	47.932	0.003
48.295	1.883	2	0	3	1.885	48.268	0.027
48.545	1.874	4	1	0	1.873	48.596	-0.051
51.817	1.763	0	4	0	1.758	52.020	-0.203
56.860	1.618	4	1	2	1.621	56.790	0.070

APPENDIX B: X-RAY DIFFRACTION SPECTRA

EXPERIMENT 5

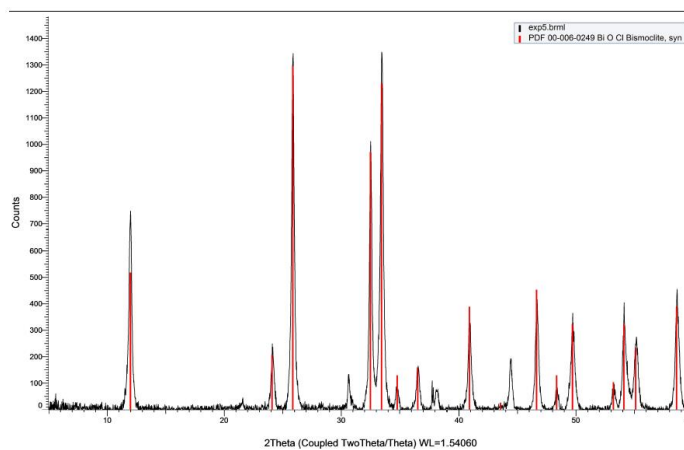


Figure 24 Exp. 5: BiOCl & CsCl (1 Cs:1 Bi), 150°C, 3hrs.

EXPERIMENT 7a

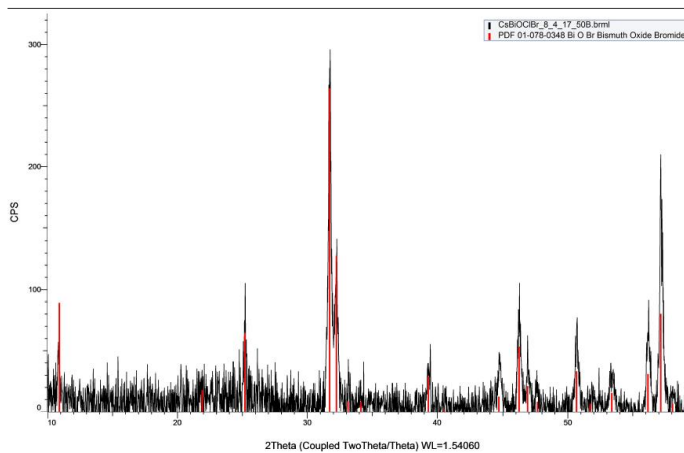


Figure 25 Exp. 7a: BiOBr & CsCl (1 Cs:1 Bi), 150°C, 3 hrs.

EXPERIMENT 7b

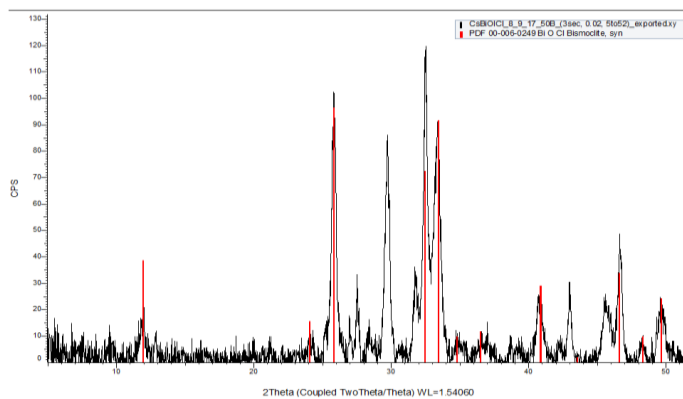


Figure 26 Exp. 7b: BiOI & CsCl (1 Cs:1 Bi) 150°C, 3 hrs.

EXPERIMENT 6

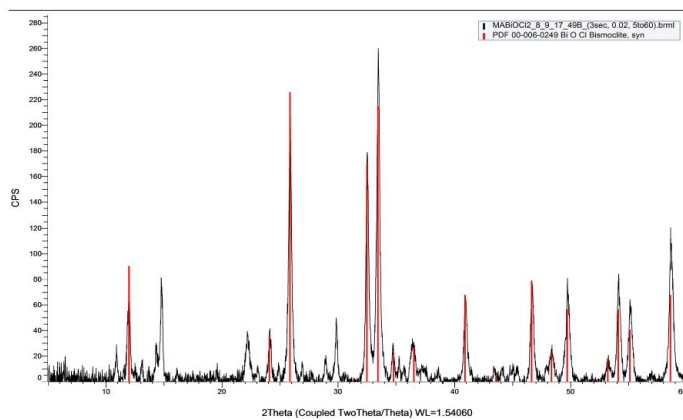


Figure 27 Exp. 6: BiOCl & MAcl (1 MA:1 Bi), 150°C, 3hrs.

EXPERIMENT 8a

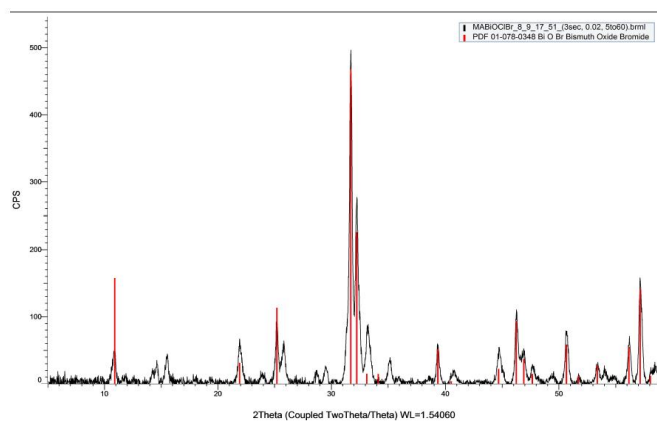


Figure 28 Exp. 8a: BiOBr & MACl (1 MA:1 Bi) 150°C, 3 hrs.

EXPERIMENT 8b

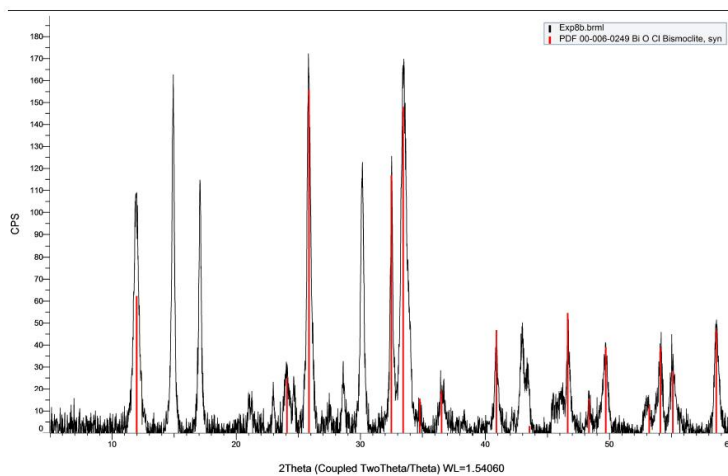


Figure 29 Exp. 8b: BiOI & MACl (1 MA:1 Bi), 150°C, 3 hrs.

EXPERIMENT 12

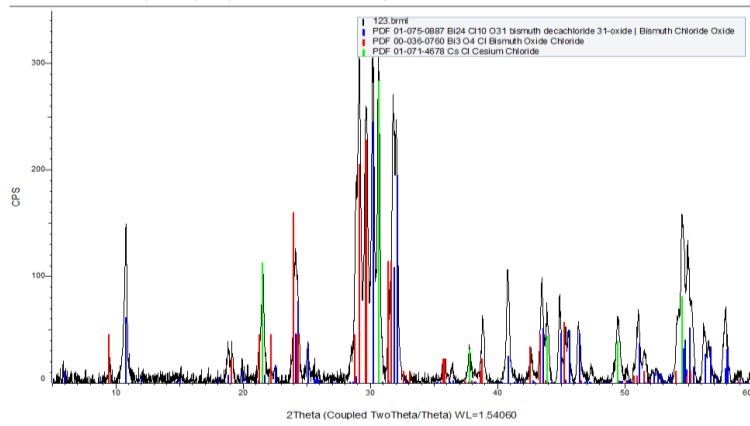


Figure 30 Exp. 12: BiOCl & CsCl, (1 Cs:1 Bi), 700°C, 22 hrs.

EXPERIMENT 17

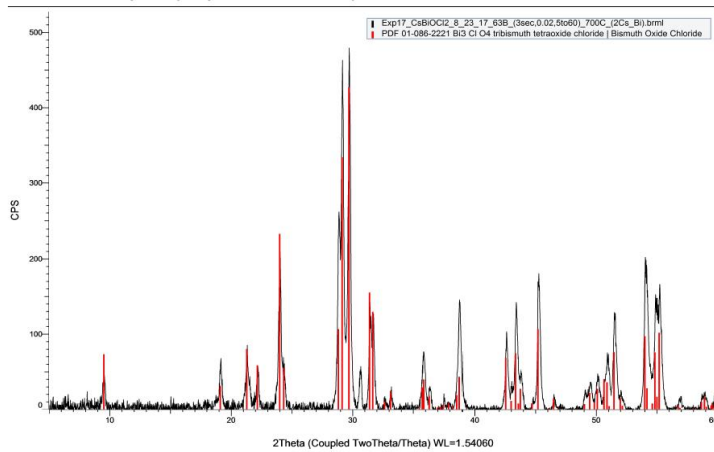


Figure 31 Exp. 17: BiOCl & CsCl, (2 Cs:1 Bi), 700°C, 21.5 hrs.

EXPERIMENT 18

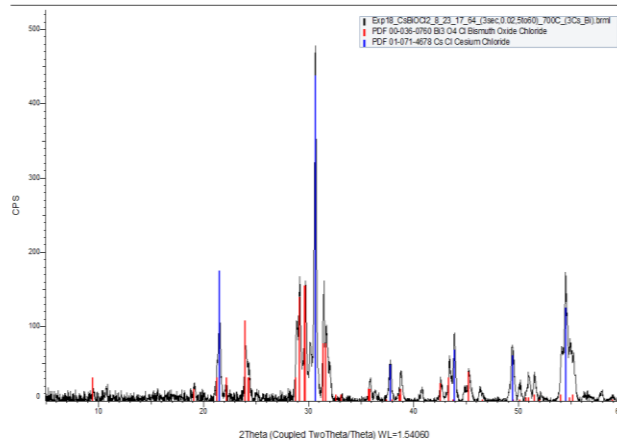


Figure 32 Exp. 18: BiOCl & CsCl, (3 Cs:1 Bi), 700°C, 21.5 hrs.

EXPERIMENT 19

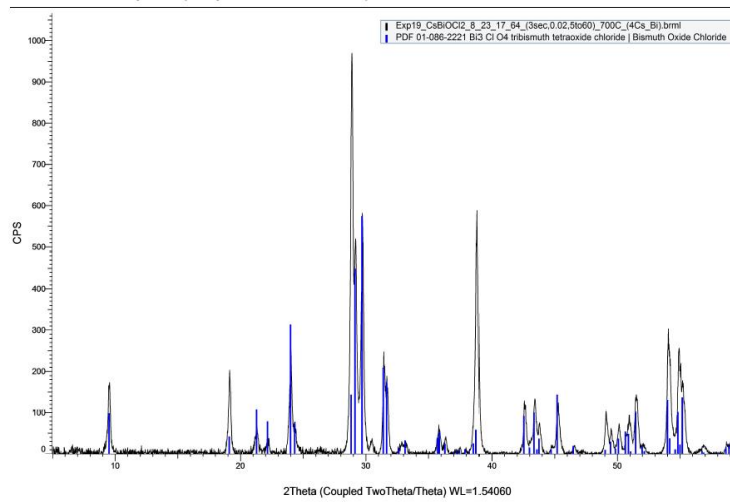


Figure 33 Exp. 19: BiOCl & CsCl, (4 Cs:1 Bi), 700°C, 21.5 hrs.

EXPERIMENT 24

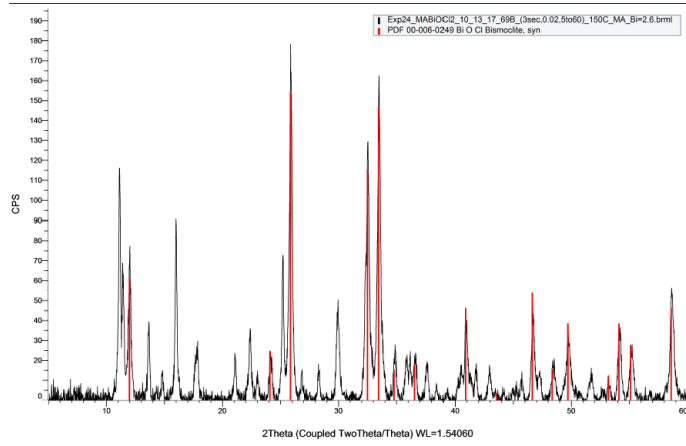


Figure 34 Exp 24: BiOCl & MAcl (2.6 MA:1 Bi), 150°C, 1hrs.

EXPERIMENT 25a

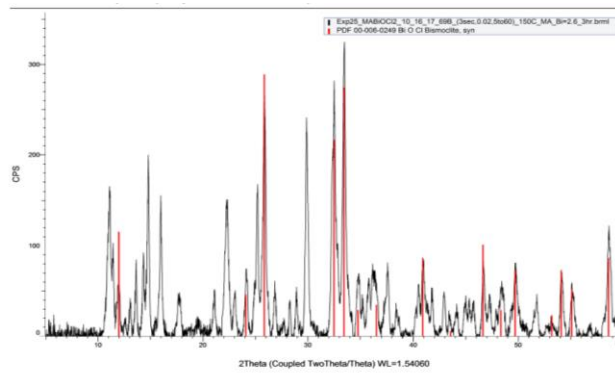


Figure 35 Exp 25a: BiOCl & MAcl (2.6 MA:1 Bi) 150°C, 3 hrs.

EXPERIMENT 25b

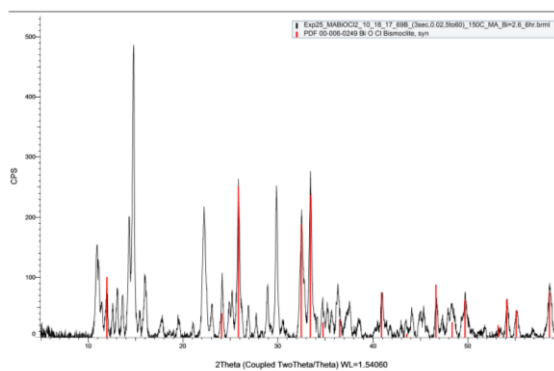


Figure 36 Exp 25b: BiOCl & MACl (2.6 MA:1 Bi), 150°C, 6 hrs.

EXPERIMENT 25c

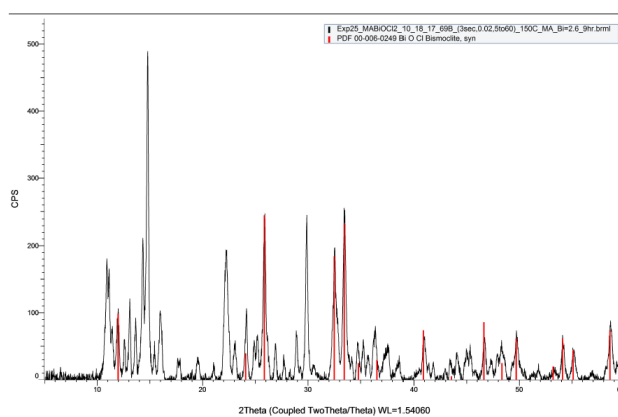


Figure 37 Exp 25c: BiOCl & MACl (2.6 MA:1 Bi), 150°C, 9 hrs.

EXPERIMENT 26a

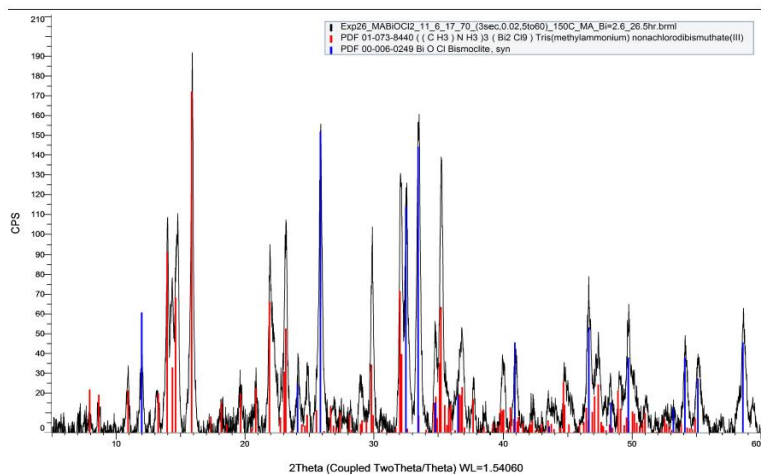


Figure 38 Exp 26a: BiOCl & MACl (2.6 MA:1 Bi) 150°C, 26.5 hrs.

EXPERIMENT 26b

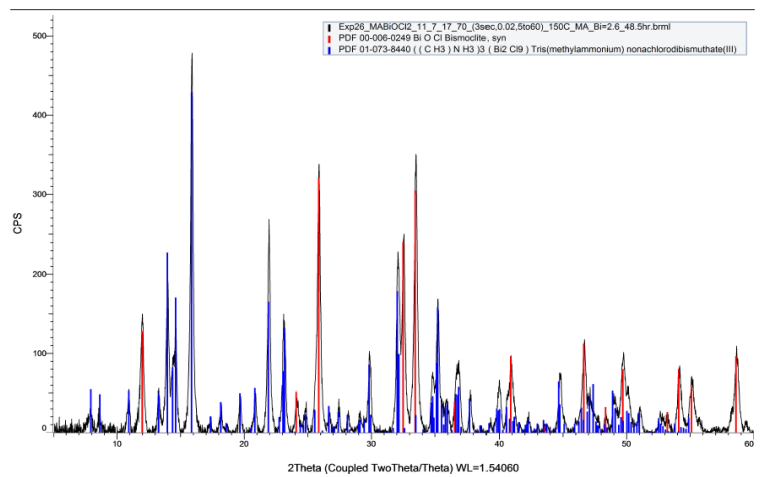


Figure 39 Exp 26b: BiOCl & MACl (2.6 MA:1 Bi), 150°C, 48.5 hrs

EXPERIMENT 27

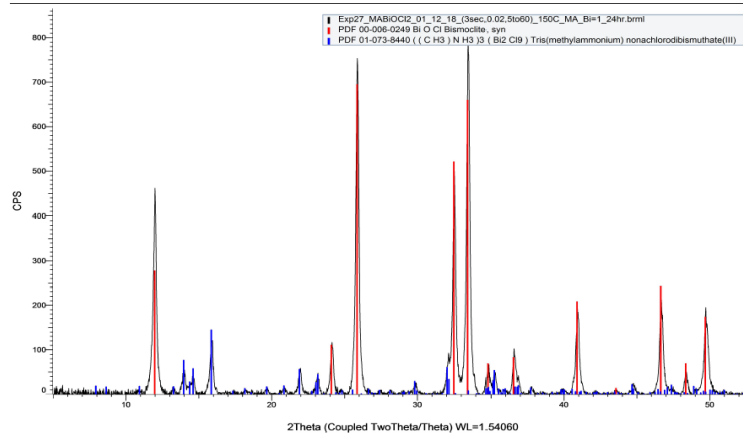


Figure 40 Exp 27: BiOCl & MAcl (1 MA:1 Bi), 150°C, 24hrs.

EXPERIMENT 28

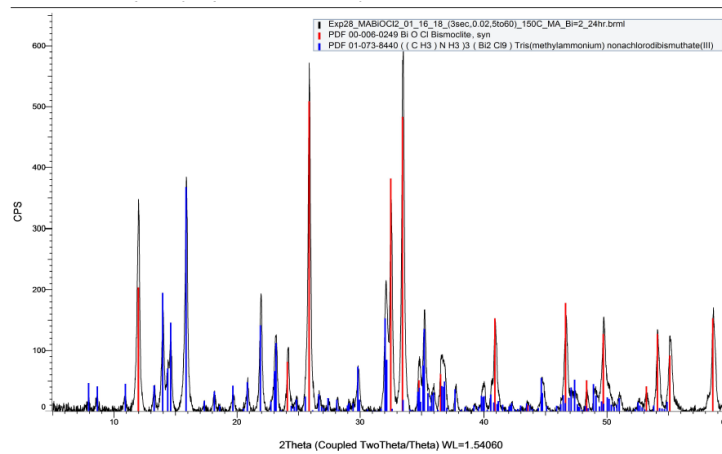


Figure 41 Exp 28: BiOCl & MAcl (2 MA:1 Bi) 150°C, 24 hrs.

EXPERIMENT 29

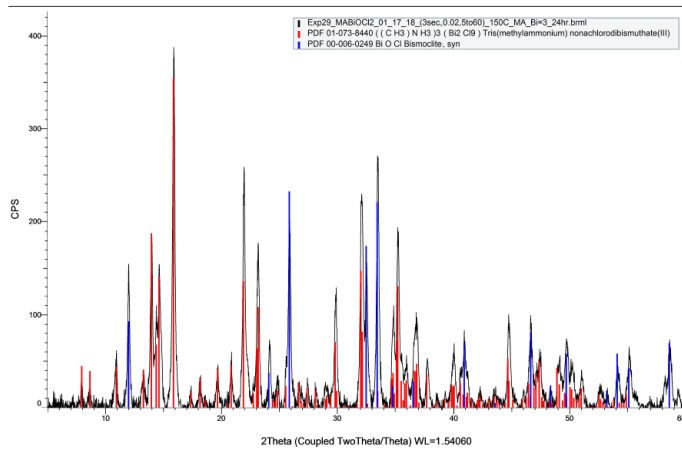


Figure 42 Exp 29: BiOCl & MAcl (3 MA:1 Bi), 150°C, 24 hrs.

EXPERIMENT 30

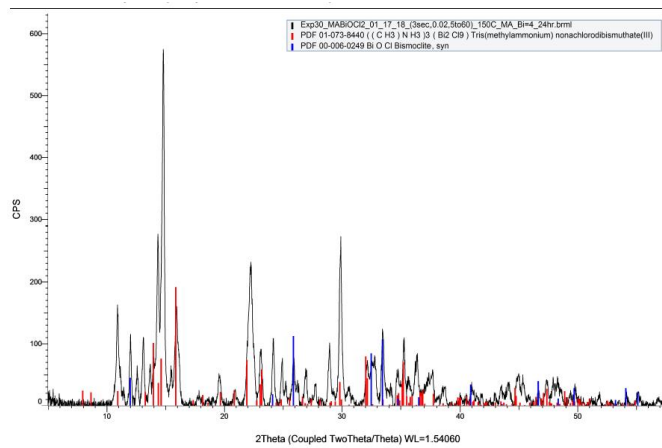
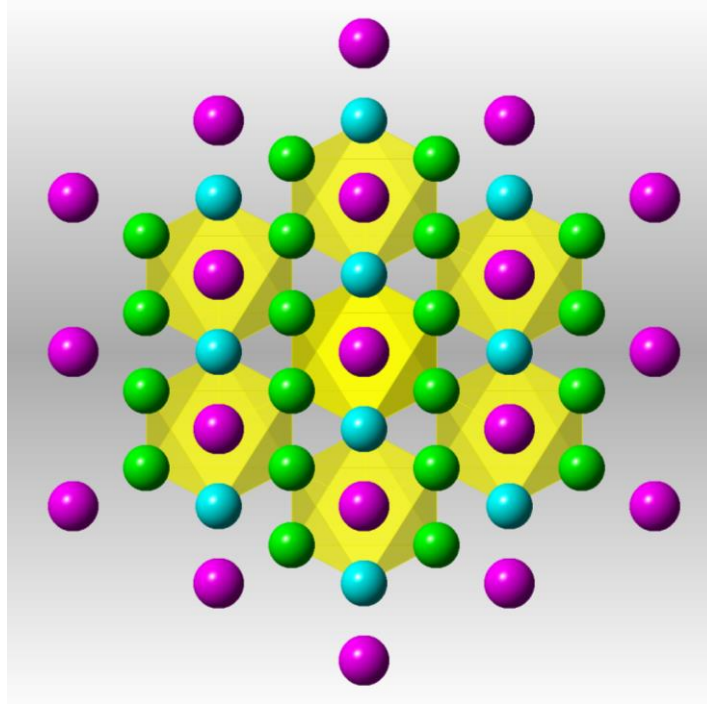


Figure 43 Exp 30: BiOCl & MAcl (4 MA:1 Bi), 150°C, 24 hrs



FIN